iScience

CellPress

Article

Genomic Profiling of Biliary Tract Cancer Cell Lines Reveals Molecular Subtypes and Actionable Drug Targets

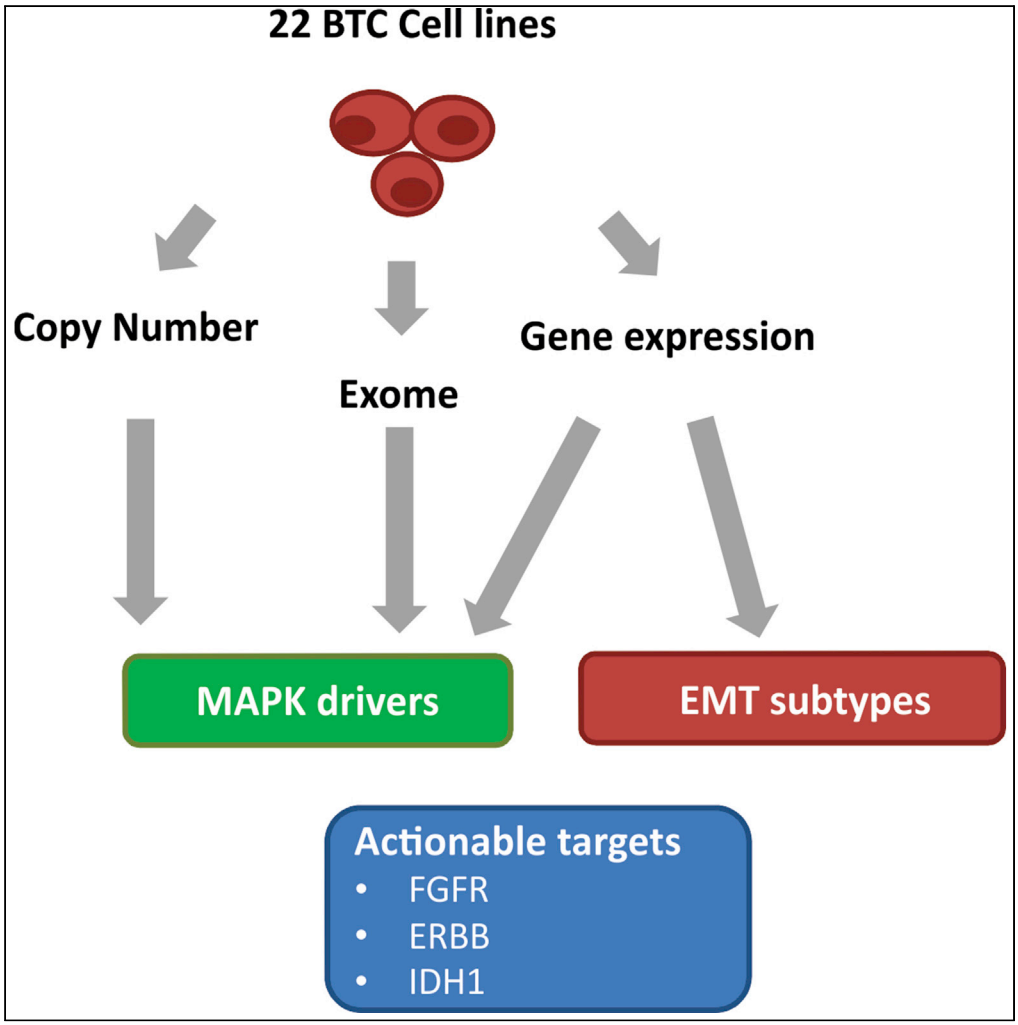

David K. Lau, Dmitri Mouradov, Wiphawan Wasenang, ..., Niall C. Tebbutt, Oliver M. Sieber, John M. Mariadason

john.mariadason@onjcri.org.au

HIGHLIGHTS

BTC cell lines harbor similar genomic alterations to primary tumors

Transcriptomic profiling of BTC cell lines identified two molecular subtypes

MAPK signaling is activated in BTC via multiple mechanisms

BTC lines with deregulated ERBB2 or FGFRs respond to specific targeted therapies

Lau et al., iScience *21*, 624–637
November 22, 2019 © 2019 The Author(s).
https://doi.org/10.1016/j.isci.2019.10.044

iScience

CellPress

Article

Genomic Profiling of Biliary Tract Cancer Cell Lines Reveals Molecular Subtypes and Actionable Drug Targets

David K. Lau,[1,2,12] Dmitri Mouradov,[3,4,12] Wiphawan Wasenang,[2,5] Ian Y. Luk,[1,2] Cameron M. Scott,[1] David S. Williams,[1,2] Yvonne H. Yeung,[1] Temduang Limpaiboon,[5] George F. Iatropoulos,[1,2] Laura J. Jenkins,[1,2] Camilla M. Reehorst,[1,2] Fiona Chionh,[1] Mehrdad Nikfarjam,[6] Daniel Croagh,[7] Amardeep S. Dhillon,[1,8] Andrew J. Weickhardt,[1,2] Toshihide Muramatsu,[9] Yoshimasa Saito,[9] Niall C. Tebbutt,[1,2] Oliver M. Sieber,[3,4,6,10,11] and John M. Mariadason[1,2,11,13,*]

SUMMARY

Biliary tract cancers (BTCs) currently have no approved targeted therapies. Although genomic profiling of primary BTCs has identified multiple potential drug targets, accurate models are needed for their evaluation. Genomic profiling of 22 BTC cell lines revealed they harbor similar mutational signatures, recurrently mutated genes, and genomic alterations to primary tumors. Transcriptomic profiling identified two major subtypes, enriched for epithelial and mesenchymal genes, which were also evident in patient-derived organoids and primary tumors. Interrogating these models revealed multiple mechanisms of MAPK signaling activation in BTC, including co-occurrence of low-activity *BRAF* and *MEK* mutations with receptor tyrosine kinase overexpression. Finally, BTC cell lines with altered *ERBB2* or FGFRs were exquisitely sensitive to specific targeted agents, whereas surprisingly, *IDH1*-mutant lines did not respond to IDH1 inhibitors *in vitro*. These findings establish BTC cell lines as robust models of primary disease, reveal specific molecular disease subsets, and highlight specific molecular vulnerabilities in these cancers.

INTRODUCTION

Biliary tract cancers (BTCs) include intra- and extrahepatic cholangiocarcinoma, gallbladder carcinomas, and ampullary carcinomas. The majority (80%–90%) of patients present with advanced disease, and each year 139,000 people die of BTC around the world, including 12,000 in the US (Charbel and Al-Kawas, 2011; Marcano-Bonilla et al., 2016). The incidence of the disease varies globally, with highest rates in northeastern Thailand and neighboring Laos and Cambodia where liver fluke infestations are endemic (Charbel and Al-Kawas, 2011). Furthermore, for reasons that are presently unknown, the incidence of intrahepatic cholangiocarcinoma is increasing in the western world (Shoda et al., 2012). Systemic chemotherapy has only modest activity in the metastatic setting, with gemcitabine plus cisplatin the standard of care, and there are currently no approved second-line or targeted therapies for BTC. Consequently, the median overall survival for these patients is approximately 12 months (Valle et al., 2010).

Initial sequencing studies aiming to characterize the genomic landscape of BTCs (Farshidfar et al., 2017; Jusakul et al., 2017; Li et al., 2014; Nakamura et al., 2015) identified a series of recurrently mutated genes, including loss-of-function mutations in the tumor suppressors *TP53* and *SMAD4* and the epigenetic modifiers *ARID1A*, *ARID2*, and *BAP1*, whereas activating mutations in *KRAS*, *PIK3CA*, and *NRAS* were the most common oncogenic events (Nakamura et al., 2015). More recent studies identified fusions involving *PRKACA* and *PRKACB* as other potential driver events (Nakamura et al., 2015), as well as mutations in *ROBO2*, *RNF43* (Ong et al., 2012), *RASA1*, *STK11*, and *MAP2K4* (Jusakul et al., 2017). These studies also identified potential therapeutically exploitable targets including mutations and amplifications of members of the ERBB family of receptor tyrosine kinases (Li et al., 2014), *IDH1* mutations (Borger et al., 2012), and *FGFR2* fusions (Arai et al., 2014); however, in many cases it remains to be determined whether these genomic alterations can be exploited for therapeutic benefit. To test this, reliable models harboring endogenous alterations in these potential targets are needed. In this regard, cell lines represent powerful models to study cancer biology and assess drug response.

[1]Olivia Newton John Cancer Research Institute, Austin Health, Level 5 ONJ Centre, 145 Studley Road, Heidelberg, Melbourne, VIC 3084, Australia

[2]School of Cancer Medicine, La Trobe University, Melbourne, VIC 3084, Australia

[3]Systems Biology and Personalised Medicine Division, The Walter and Eliza Hall Institute of Medical Research, Melbourne, VIC 3052, Australia

[4]Department of Medical Biology, The University of Melbourne, Melbourne, VIC 3052, Australia

[5]Centre for Research and Development of Medical Diagnostic Laboratories, Khon Kaen University, Khon Kaen 40002, Thailand

[6]Department of Surgery, University of Melbourne, Melbourne, VIC 3084, Australia

[7]Department of Surgery, Monash Medical Centre, Monash University, Melbourne, VIC 3168, Australia

[8]School of Medicine, Deakin University, Geelong, VIC 3216, Australia

[9]Division of Pharmacotherapeutics, Keio University Faculty of Pharmacy, Tokyo 105-8512, Japan

[10]Department of Biochemistry & Molecular Biology, Monash University, Melbourne, VIC 3800, Australia

Continued

This is an open access article under the CC BY-NC-ND license (http://creativecommons.org/licenses/by-nc-nd/4.0/).

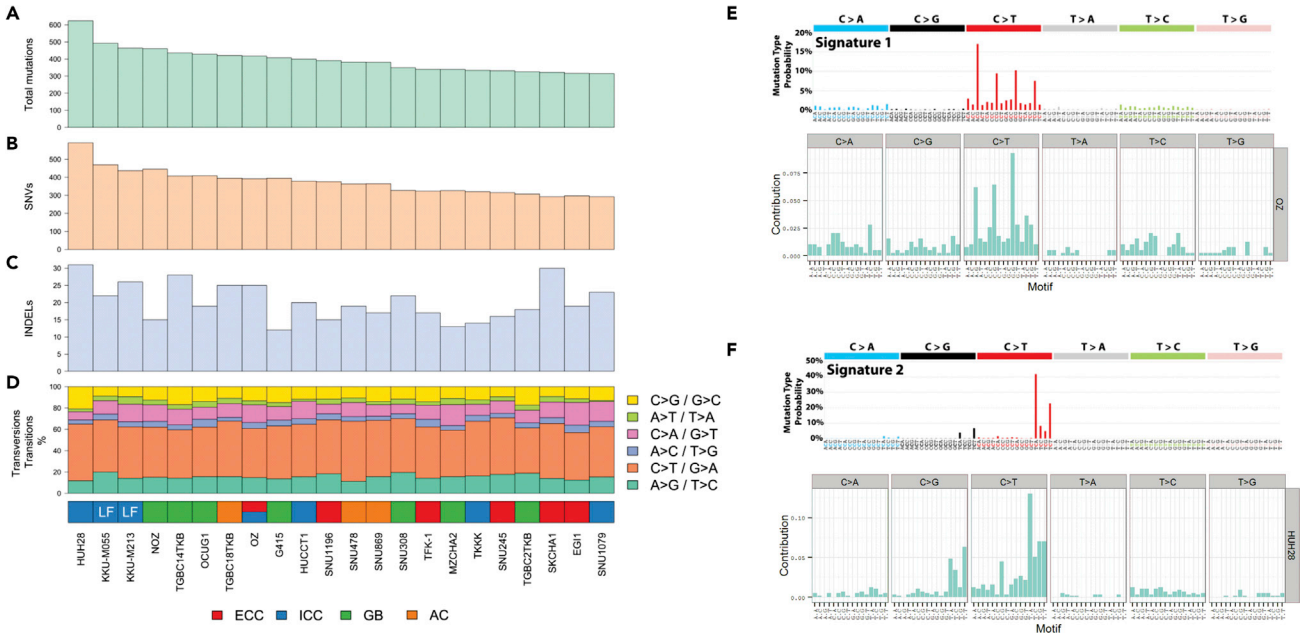

Figure 1. Mutation Burden and Mutational Signatures in 22 Biliary Cancer Cell Lines

(A) Counts of total mutations, (B) SNVs, and (C) InDels in BTC cell lines.

(D) Percentage of nucleotide transitions and transversions.

(E and F) Representative cell lines harboring (E) mutational signature 1 (OZ cells) and (F) mutational signature 2 (HuH28 cells). ECC, extrahepatic cholangiocarcinoma; ICC, intrahepatic cholangiocarcinoma; GB, gallbladder carcinoma; AC, ampullary cancer; LF, liver-fluke-associated intrahepatic cholangiocarcinoma.

Although a number of BTC cell lines have been established, their genomic profiles have not been extensively characterized and compared with that of primary BTCs. In this study, we comprehensively profiled 22 BTC cell lines by exome sequencing, copy number analysis, and RNA-seq analysis. We found that the most frequently observed genomic alterations in primary BTCs are preserved in cell lines validating their use as accurate model systems to study this disease. In addition, we identified two distinct molecular subsets of BTC cell lines that differ in expression of EMT genes and importantly demonstrate that these signatures are also evident in patient-derived organoid models and primary BTCs. We also demonstrate that the MAPK signaling pathway is deregulated by multiple mechanisms in BTC and identify a number of potential actionable drug targets for this disease.

RESULTS

Exome Sequencing of Biliary Cancer Cell Lines

A panel of 22 BTC cell lines derived from tumors from distinct anatomical locations within the biliary tree was assembled from international cell repositories and individual investigators (Table S1). The panel comprised the majority of BTC lines described in the literature (Homma et al., 1987, 1988; Knuth et al., 1985; Koyama et al., 1980; Ku et al., 2002; Kusaka et al., 1988; Miyagiwa et al., 1989; Yamada et al., 1997), including two cell lines, KKU-M055 and KKU-M213, derived from liver-fluke-associated intrahepatic cholangiocarcinoma (Obchoei et al., 2011; Tepsiri et al., 2005).

The total number of mutations (SNVs + InDels) ranged from 315 to 623 (mean 394) across the cell lines (Figures 1A–1C and Table S2). The average frequency of Indels in cell lines (0.27 InDels/Mb, range 0.16–0.42 InDels/Mb) was similar to that observed in primary cancers (0.32 InDels/Mb). Comparatively, the average mutation rate for cell lines (5.0 SNVs/Mb, range 3.9–7.9 SNVs/Mb) was higher than that observed in primary BTCs (mean 2.6 SNVs/Mb). No hypermutated cell lines (>25 mutations/Mb) were identified in the panel, consistent with the low frequency (5%) of hypermutated cases in primary BTCs (Nakamura et al., 2015).

The dominant somatic substitution pattern observed in primary BTCs are C > T/G > A transitions that are enriched at CpG dinucleotides, followed by T > C/A > G transitions and C > A/T > G transversions

[11]Department of Medicine, The University of Melbourne, Melbourne, VIC 3052, Australia

[12]These authors contributed equally

[13]Lead Contact

*Correspondence: john.mariadason@onjcri.org.au

https://doi.org/10.1016/j.isci.2019.10.044

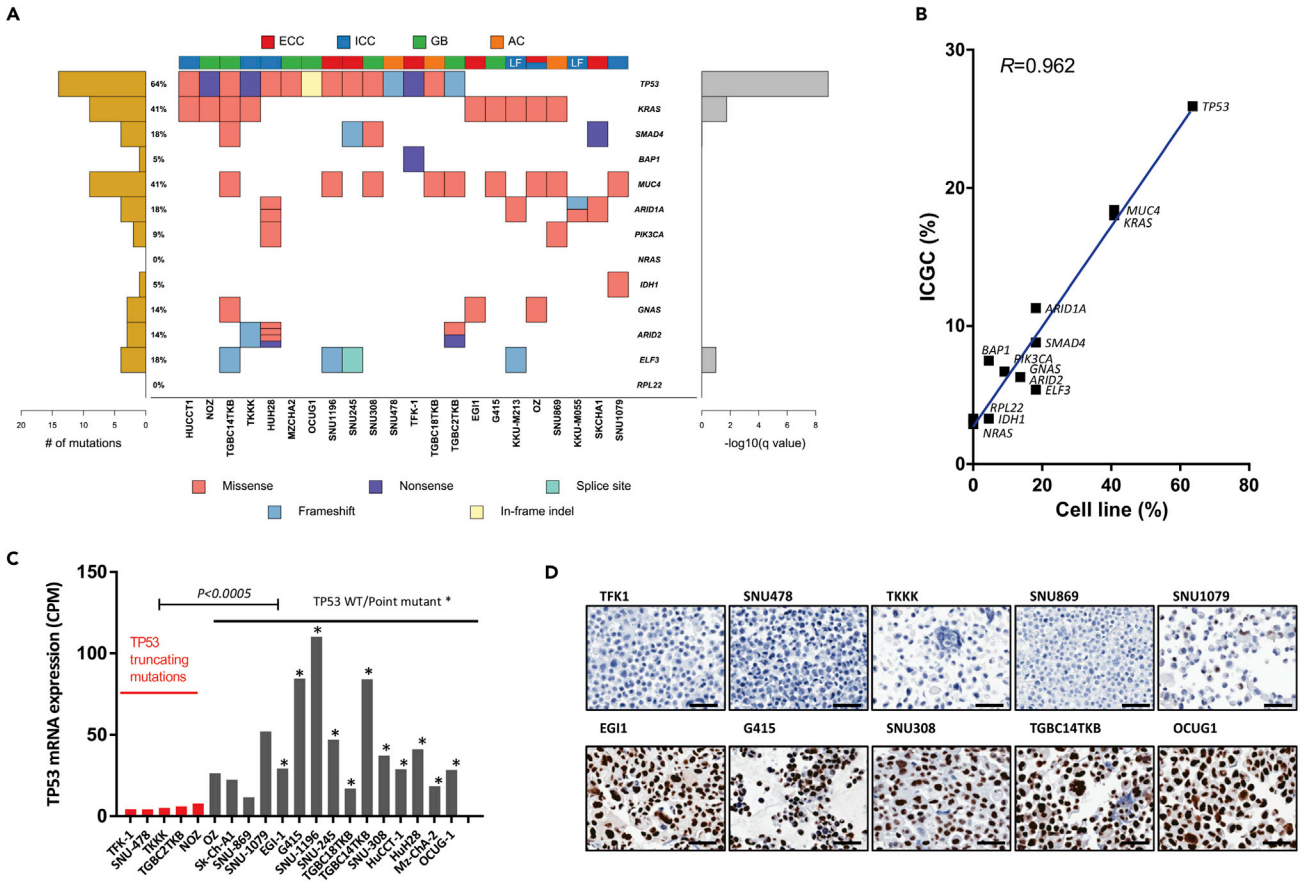

Figure 2. Comparison of the Mutation Landscape of BTC Cell Lines with Primary BTCs and Validation of *TP53* Mutation Status

(A) Oncoplot of the most significantly mutated genes in primary BTC.

(B) Pearson's correlation of the frequency of mutations in cell lines compared with primary cancers from the ICGC (International Cancer Genomics Consortium). ECC, extrahepatic cholangiocarcinoma; ICC, intrahepatic cholangiocarcinoma; GB, gallbladder carcinoma; AC, ampullary cancer; LF, liver-fluke-associated intrahepatic cholangiocarcinoma.

(C) TP53 mRNA expression in *TP53* wild-type and mutant BTC cell lines determined by RNA-seq. Groups were compared using an unpaired t test.

(D) TP53 protein expression determined by immunohistochemistry in *TP53* wild-type and mutant BTC cell lines. Scale bar 50 μM.

(Alexandrov et al., 2013; Nakamura et al., 2015). This pattern is similar in fluke- and non-fluke-derived tumors (Chan-On et al., 2013). A similar distribution of somatic substitution patterns was observed in BTC cell lines, with C > T (0.49 ± 0.03) transitions as the dominant pattern observed, followed by T > C (0.15 ± 0.02) transitions and C > A transversions (0.14 ± 0.04) (Figure 1D).

In primary BTC, two predominant mutational signatures have been identified: (A/C/G)CG>(A/C/G)TG previously defined as Signature 1 by Alexandrov et al. (Alexandrov et al., 2013), which is the result of an endogenous mutational process initiated by spontaneous deamination of 5-methylcytosine, and TC(A/C/T) >TG(A/C/T) and TCN > TTN, which is similar to the previously defined APOBEC-associated signature (Signature 2) (Alexandrov et al., 2013). Although the predominant signature in BTC cell lines was Signature 1 (Figure 1E), we identified one cell line (HuH28, intrahepatic) with the classical APOBEC signature (Figure 1F), which was also the cell line harboring the highest mutational load.

Comparison of the Most Frequently Mutated Genes in Primary BTCs and BTC Cell Lines

To determine if the genes most frequently mutated in primary BTCs are reflected in BTC cell lines, we compared the frequency of mutations with that reported by Nakamura et al. in which 13 significantly mutated genes were identified from sequencing 260 primary BTCs (Nakamura et al., 2015). Compared with primary disease, the mutational frequency of several known oncogenes and tumor suppressor genes

including *TP53* (25.9% vs 63.6%), *KRAS* (18.0 vs 40.9%), and *SMAD4* (8.8% vs 18.2%) were higher in cell lines (Figure 2A). Nevertheless, we observed a strong correlation between the most frequently mutated genes in primary cancers and cell lines (Pearson's $R = 0.962$), demonstrating that although cell lines have a higher mutational frequency of major oncogenes and tumor suppressor genes, the relative proportion of these mutations is similar to that observed in primary disease (Figure 2B).

Functional Validation of Specific Mutations in BTC

To validate the functionality of specific mutations, we examined corresponding mRNA expression of genes harboring truncating mutations by analysis of RNA-seq data generated for each cell line. As expected, cell lines harboring truncating *TP53* mutations had significantly lower *TP53* mRNA expression compared with *TP53* wild-type cell lines or cell lines harboring *TP53* point mutations (Figure 2C). Furthermore, immunohistochemical staining of the cell lines revealed high TP53 protein expression in mutant cell lines compared with wild-type lines or lines harboring truncating mutations (Figure 2D). Similarly, the single cell line harboring a homozygous inactivating mutation in *BAP1* (TFK-1) had the lowest level of BAP1 mRNA expression among the cell lines (Figure S1A). We also identified three cell lines harboring mutations in the WNT pathway (KKU-M055, *APC* frameshift; TGBC18TKB, *CTNNB1 T41A*; and SNU-869, *CTNNB1 S45P*). KKU-M055 cells also harbored a deletion of *APC* (Chr5 q22.2) consistent with loss of heterozygosity. As expected, these three lines had markedly higher Wnt reporter (TOPFLASH) activity, and expression of the Wnt target gene, *AXIN2*, compared with wild-type lines (Figures S2A and S2B). Notably, inactivating mutations in the E3 ubiquitin ligase *RNF43* have also been reported to enhance canonical Wnt signaling due to failure to degrade FZD receptors on the cell surface (Koo et al., 2012), and we identified one cell line, Sk-ChA-1, harboring a biallelic inactivating *RNF43* mutation, which also had low levels of *RNF43* mRNA expression (Figure S1B). Surprisingly, however, TOPFLASH activity and Wnt target gene expression was not elevated in this line (Figures S2A and S2B), and Sk-ChA-1 cells were not preferentially sensitive to exogenous Wnt ligand (Figure S2C), collectively indicating that the inactivating *RNF43* mutation in this line does not activate the Wnt pathway.

DNA Copy Number Changes and Identification of Focal Regions of Amplification and Deletion in BTC Cell Lines

To investigate changes in DNA copy-number, we utilized Illumina OmniExpress SNP arrays. The most commonly deleted genomic regions were chromosome *8p* and chromosome *18*, whereas the most commonly gained regions were *5p, 7p, 17q,* and chromosome *20*. We also identified focal regions significantly altered by DNA copy-number alterations in cell lines using GISTIC. Significantly amplified genes across the cell lines were *KRAS* (*12p12.1*), *SLCO1B* (*12p12.2*), *ALG10* (*12p11.1*), *hsa-mir-720/hsa-mir-1263/BCHE* (*3q26.1*), and *POU5F1B* (*8q24.21*), and significantly deleted regions were *CDKN2A/B* (*9p21.3*), *FHIT* (*3p14.2*), *WWOX* (*16q23.1*), *MACROD2* (*20p12.1*), and *TPRG1* (*3q28*) (Figure 3A).

We also performed an analysis in which we determined the extent of overlap of the 33 homozygously deleted and 22 focally amplified genes identified in >2 primary BTCs by Nakamura et al. (Nakamura et al., 2015). Of the 33 homozygous deleted genes, 16 (47%) were also deleted in one or more cell line. All of these genes were located at chromosome *9p21.3* and included *CDKN2A* and *CDKN2B*. Confirming the deletion of *CDKN2A* and the adjacently located *CDKN2B*, mRNA expression of these genes was significantly lower in cell lines harboring homozygous deletions (Figure 3B). In comparison, 20 of the 22 amplified genes identified in primary disease were found to be also amplified in at least one BTC cell line (copy number ≥ 5), of which five genes (22%) had copy numbers ≥ 7 in one or more cell lines (*MYC, YEATS4, CCND3, IKBKB, KRAS*) (Tables S3 and S4). Notably, four of these five focally amplified genes displayed corresponding increases in mRNA expression (Figure 3C).

Unsupervised Clustering of Cell Lines Based on Gene Expression Identifies Two Major Subgroups that Differ in Epithelial and Mesenchymal Characteristics

We next performed RNA-seq analysis on the cell lines. Unsupervised clustering based on expression of all genes separated the cell lines into two major groups, comprising 7 and 13 cell lines (Figure 4A). Gene set enrichment analysis of the 411 genes differentially expressed between these groups identified the hallmarks epithelial-mesenchymal transition (EMT), mitotic spindle, and hypoxia with the most significant enrichment scores in the smaller cluster, whereas cholesterol homeostasis, IFN alpha and gamma response, and early and late estrogen response were significantly enriched in the larger cluster (Figure 4B). Consistent with enrichment of the EMT hallmark, expression of mesenchymal genes *CTGF, FLNA, FN1, TGFβ1,* and *ZEB1* were higher in the smaller cluster (mesenchymal cluster), whereas expression of multiple

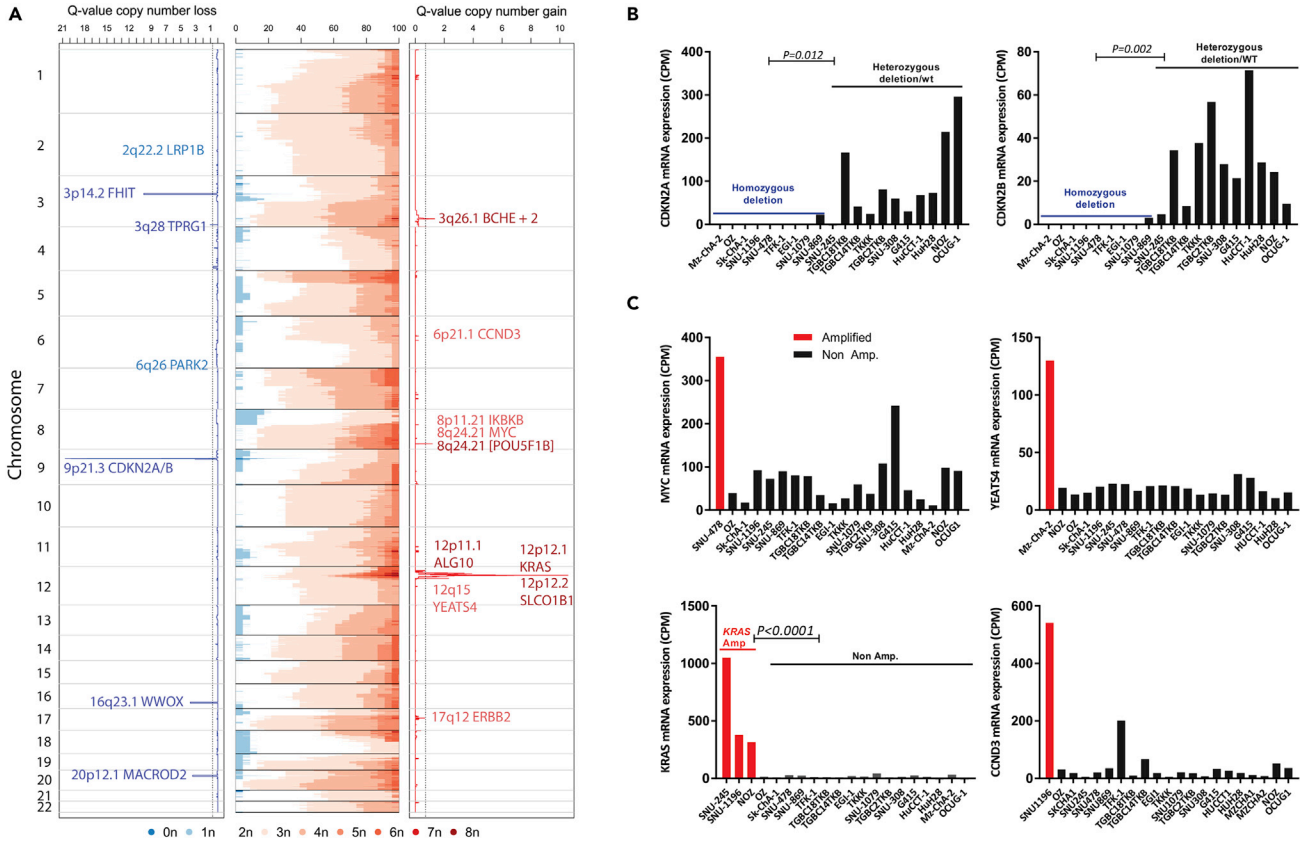

Figure 3. Genome-Wide DNA Copy Number Alterations in BTC Cell Lines

(A) DNA copy-number gains and losses in 22 BTC cell lines deduced using OmniExpress arrays and the OncoSNP tool for characterizing copy number alterations. Significant regions of chromosomal loss (dark blue) and gain (dark red) deduced using GISTIC2.0. Focally deleted and amplified genes in specific cell lines are indicated in light blue and red, respectively.

(B and C) Corresponding mRNA expression of representative (B) deleted and (C) amplified genes determined by RNA-seq.

drivers (*ELF3, KLF5, EHF*) and markers of epithelial differentiation (*CDH1, EPCAM, KRT19, KRT8, VILL*) and tight junction components (*CGN, CRB3, CLDN4, CLDN7, F11R, TJP3*) were more highly expressed in the "epithelial cluster" (Figure 4A). Notably, four out of seven lines in the mesenchymal cluster were derived from metastatic gallbladder cases. To determine if these transcriptional differences translated to histological differences, representative cell lines from each cluster were grown as xenografts. All three lines from the mesenchymal cluster grew as poorly differentiated tumors with no glandular structure, whereas the three lines from the epithelial cluster grew as moderately differentiated tumors with clear evidence of glandular morphology (Figure 4C). Furthermore, the majority of cell lines from the mesenchymal cluster grew primarily as single cells or with spindle-like morphology *in vitro*, compared with cell lines from the epithelial cluster where many grew in patches of closely adhered cells (Figures S3 and S4).

To determine if these signatures were also evident in patient-derived organoid (PDO) models, we analyzed microarray data available from four recently generated PDOs, three of which were derived from well-to-moderately differentiated tumors (19T, 1T, 24T) and one that was derived from a moderately-to-poorly differentiated tumor (9T) (Saito et al., 2019). Expression of the epithelial genes *CLDN4, EPCAM, TJP3,* and *KRT19* was highest in the well-to-moderately differentiated organoids, whereas expression of the mesenchymal genes *TGFB1, ZEB1, FN1,* and *CALD1* was highest in the 9T organoid (Figure 4D), demonstrating the cell-line-derived gene expression signature of tumor histology is also evident in organoid models of the disease.

Finally, to determine if primary BTCs harboring these signatures could be identified, 35 primary BTCs profiled by the TCGA were clustered with the cell lines based on the EMT signature. This analysis identified two

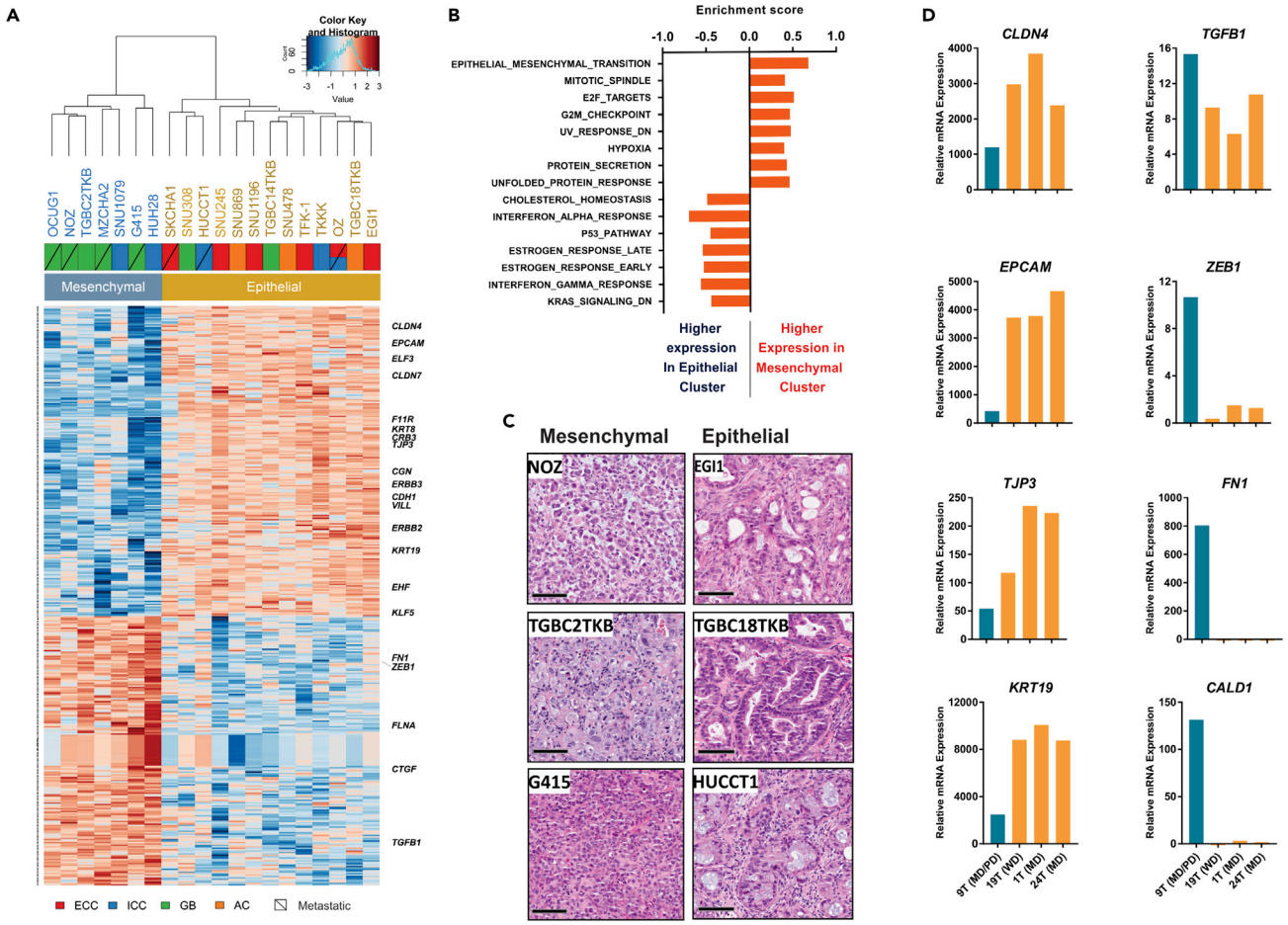

Figure 4. Basal Gene Expression Profiles of BTC Cell Lines Determined by RNA-seq Analysis

(A) Unsupervised cluster analysis of 20 BTC cell lines based on basal level of expression of all genes determined by RNA-seq analysis. Heatmap shows the 411 genes with significant differential expression between the two clusters. RNA-seq analyses of KKU-M055 and KKU-M213 cells were performed at a later time by a different method and were not included in the analysis due to batch effects.

(B) Gene set enrichment analysis of 411 differentially expressed genes between the two clusters.

(C) Histology of representative BTC cell lines from epithelial and mesenchymal clusters following growth as xenografts. Scale bar 100 μM.

(D) Expression of epithelial and mesenchymal genes in patient-derived biliary cancer organoids from patients with well-differentiated (WD), moderately differentiated, (MD) or moderate-to-poorly differentiated (MD/PD) tumors. Values shown are from microarray analyses of these organoids (GSE112408).

primary BTCs that clustered with the mesenchymal lines and eight primary tumors that clustered with the epithelial lines (Figure S5). Notably, examination of the histopathology of the primary tumors in the mesenchymal cluster confirmed that case TCGA-ZU-A8S4 was a sarcomatoid carcinoma showing spindle cell (mesenchymal) morphology with no evidence of gland formation, whereas case TCGA-W5-AA2H showed some gland formation but also a high degree of tumor budding, forming small clusters of spindle shaped tumor cells (Figure S6). Comparatively, all eight primary cases that clustered with the epithelial lines showed clear evidence of gland formation and epithelioid cell morphology, without spindle cells or tumor budding (Figure S6).

Investigation of Actionable Genetic Alterations in BTC

IDH1^{R132C} *Mutation*

We identified one cell line (SNU-1079, intrahepatic) harboring an *IDH1* ^{R132C} hotspot mutation, which was confirmed using Sanger sequencing (Figure S7A inset). Consistent with the neomorphic advantage conferred by this mutation (Ward et al., 2010), levels of the oncometabolite R-2-hydroxy-glutarate (2-HG) were markedly elevated in culture medium and cell pellets from this line (Figure S7A). Treatment of

SNU-1079 cells with the mutant IDH1 inhibitor AGI-5198 significantly decreased 2-HG accumulation (Figure S7B); however, neither AGI-5198 nor the clinically used derivative AG-120 (ivosidenib) inhibited proliferation of this line (Figure S7C). To determine whether similar effects occurred in PDOs, we determined the effect of AG-120 in the 9T PDO, generated from a patient with an *IDH1*^{R132L} mutant intrahepatic cholangiocarcinoma. As observed in SNU-1079 cells, AG-120 failed to inhibit growth of the *IDH1*^{R132L} organoid, with instead a modest but significant increase in cell proliferation observed (Figure S7D).

Recent studies have suggested that mutant *IDH* may promote cholangiocarcinoma development by suppressing *HNF4A* expression and blocking hepatocyte differentiation (Saha et al., 2014), and initial data from clinical trials of AG-120 in *IDH1* mutant cholangiocarcinoma have reported an upregulation of liver-specific genes in serial biopsy samples (Ishii et al., 2018). However, treatment of SNU-1079 cells with AGI-5198 or AG-120 failed to increase expression of *HNF4A* or other hepatocyte markers (*MGST1, CYP27A1, ALB*) or markers of epithelial (*EPCAM*) or mesenchymal (*VIM*) transition (Figure S7E). Finally, as increased benefit of *IDH1* mutant BTCs to chemotherapy was recently reported (Molenaar et al., 2018), we assessed the sensitivity of this line to gemcitabine. Although SNU-1079 cells were not exquisitely sensitive to gemcitabine, it ranked among the more sensitive lines (Figure S7F). However, pre-treatment of SNU-1079 cells with AGI-5198 did not further enhance sensitivity, suggesting the sensitivity of *IDH*-mutant tumors to chemotherapy may not be directly related to elevated 2-HG levels (Figure S7G).

ERBB2 Mutation and Amplification

Mutations in the ERBB family of receptor tyrosine kinases, particularly *ERBB2* and *ERBB3,* occur in ~10% of BTCs and we identified one cell line, TGBC18TKB, which carried two hotspot mutations in *ERBB2* (*S310F* and *R678Q*) (Figure 5A), which have been previously reported in primary BTC (Li et al., 2014). Notably, mRNA expression of ERBB2 was also highly elevated in TGBC18TKB cells (Figure 5B). We also identified a second cell line, TKKK, with highly elevated levels of ERBB2 mRNA (Figure 5B). Copy number analysis of this cell line revealed an amplification in *ERBB2* (Figure 3A), which was confirmed by qRT-PCR and *in situ hybridization* (Figures 5C and 5D). Importantly, both TGBC18TKB and TKKK cells were markedly more sensitive to the ERBB2 inhibitors lapatinib and AZD8931 compared with WT lines, establishing these mutations as potential drug targets in BTC (Figures 5E and 5F).

ERK-MAPK Signaling Is Activated by Multiple Mechanisms in BTC Cell Lines

Integration of the exome sequencing data and DNA copy number analysis revealed multiple mechanisms of ERK/MAPK pathway activation in BTC cell lines. Specifically, *KRAS* mutations were identified in 8/22 cell lines, whereas amplification of *KRAS* was observed in three cell lines of which one line (NOZ) also harbored a *KRAS* mutation (Table S5). In addition, we identified two cell lines harboring low-activity *BRAF* mutations (TGBC18TKB, *BRAF*$^{I581L,\ N582T}$, and Sk-Ch-A1, *BRAF*^{D594T}) (Table S5). Unlike activating *BRAF* mutations (V600E), these mutants act as amplifiers of RAS signaling and often coexist with other forms of RAS activation (Yao et al., 2017). The identification of *ERBB2* hotspot mutations in TGBC18TKB cells (Figure 5A) is consistent with this mechanism. Similarly, we identified a truncating mutation in *RASA1* in Sk-Ch-A1 cells (Table S2 and Figure S1), which encodes the Ras GTPase-activating protein p120-RasGAP, which suppresses RAS signaling by converting RAS to the inactive GDP-bound form (Lapinski et al., 2007).

We also identified one cell line (KKU-M055) with a K57N mutation in *MAP2K1* (*MEK1*), which has been previously observed in lung adenocarcinoma and melanoma (Figure 6A). As with low-activity *BRAF* mutations, *MAP2K1*^{K57N} was recently classified as a class II MEK mutant, which is partially dependent on upstream RAF to drive ERK signaling and likely acts as an amplifier of RAS signaling (Gao et al., 2018). Notably, compared with *MEK*^{WT} G415 cells, *MEK*^{K57N} mutant KKU-M055 cells were highly resistant to growth inhibition or signaling inhibition induced by the allosteric MEK inhibitor trametinib or the ERK inhibitor SCH772984 (Figures 6B–6E). Time course experiments also demonstrated that SCH772984 increased levels of active CRAF (pCRAF S338) in both *MAP2K*^{K57N} mutant and WT cell lines (Figure 6F), which is an expected effect of this drug due to relief of ERK-mediated inhibitory phosphorylation of CRAF (Dougherty et al., 2005). However, although pERK levels remained suppressed in MEK^{WT} G415 cells after 6 h, they were strongly reactivated in *MEK*^{K57N} mutant KKU-M055 cells, consistent with the *MAP2K*^{K57N} acting to amplify BRAF/MAPK/ERK signaling (Figure 6F).

The role of *MAP2K*^{K57N} as an amplifier of RAS signaling suggested KKU-M055 cells may also harbor alterations in upstream components of the RAS/MAPK pathway. As no mutations in *RAS, BRAF, NF1,* and *RASA1*

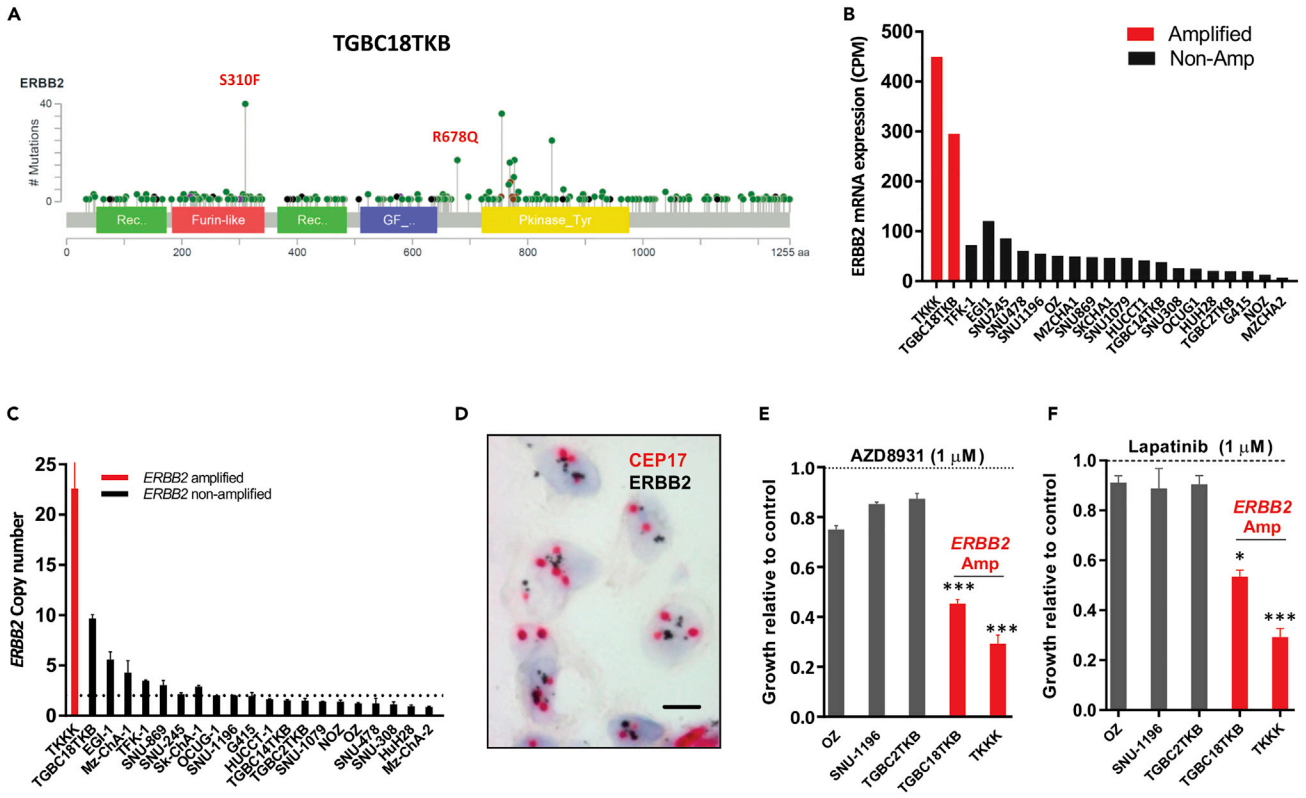

Figure 5. Characterization of *ERBB2* Mutant and Amplified BTC Cell Lines

(A) Location of two *ERBB2* mutations in TGBC18TKB cells highlighted in red. Mutation plot from cBioPortal. Lollipops designate mutation points.

(B) *ERBB2* mRNA expression in BTC cell lines determined by RNA-seq.

(C and D) Validation of *ERBB2* amplification in TKKK cells by (C) q-RT-PCR–based DNA copy number analysis and (D) *in situ* hybridization (scale bar 5 μM). Values shown in C are mean ± SEM of a single sample assayed in technical triplicate.

(E and F) Effect of the ERRB2 inhibitors (E) AZD8931 and (F) lapatinib on proliferation of *ERBB2* mutant/amplified and WT BTC cell lines. Cells were treated with drug for 72 h and cell proliferation determined by MTS assay. Values shown are mean ± SEM of a single experiment analyzed in quadruplicate. Similar results were obtained in two independent experiments. $^{**}p < 0.005$, $^{***}p < 0.0005$ compared with untreated controls, unpaired t test.

were present, we investigated mRNA expression of the major receptor tyrosine kinases (RTKs), which revealed marked overexpression of FGFR1 in this cell line (Figure 7A). Furthermore, KKU-M055 cells were highly sensitive to the FGFR inhibitors BGJ398 and erdafitinib both *in vitro* and *in vivo* (Figures 7B–7E), suggesting proliferation of KKU-M055 cells is driven by FGFR1, with the MEK^{K57N} mutation likely acting to amplify FGFR-driven MAPK signaling.

FGFR3 and FGFR4

Finally, we utilized the RNA-seq data to perform an outlier analysis in order to identify other cell lines that expressed exceptionally high levels of targetable receptor tyrosine kinases. This approach identified high levels of *FGFR3* and *FGFR4* mRNA in Mz-ChA-2 cells (Figures 7F and 7G). Interrogation of the signaling components downstream of FGFR in this cell line also revealed a focal low-level amplification of the FGFR docking protein *FRS2* (Figure 7H) (Turner and Grose, 2010). Treatment of Mz-ChA-2 cells with the FGFR inhibitors BGJ398 and erdafitinib induced exquisite sensitivity to both inhibitors compared with non-overexpressing lines (Figures 7I and 7J).

DISCUSSION

BTCs are a genomically heterogeneous group of cancers featuring a substantial number of low prevalence mutations. In this study, we profiled the genomic landscape of 22 BTC cell lines derived from various anatomical locations in the biliary tract and demonstrate that the most commonly mutated driver genes,

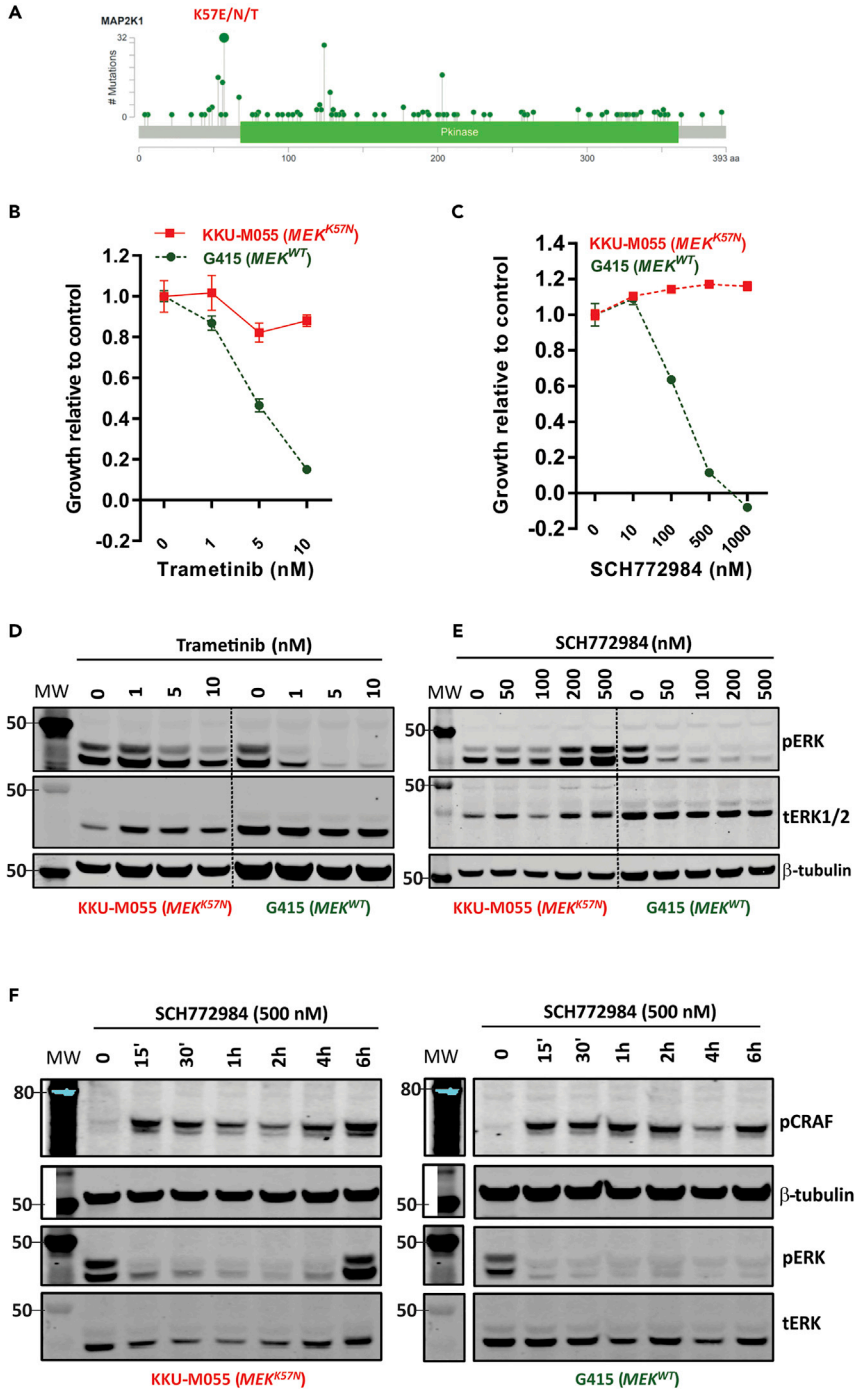

Figure 6. Characterization of *MEK1*^{K57N} Mutant Cell Line

(A) Mutation plot from cBioPortal showing location and frequency of occurrence of *MEK*^{K57N} mutation in human cancers. Lollipops designate mutation points.

(B and C) MTS assays of a *MEK*^{K57N}-mutant (KKU-M055) and a *MEK*^{WT} cell line (G415) treated with (B) the MEK inhibitor trametinib or (C) the ERK inhibitor SCH772984 for 72 h. Values shown are mean ± SEM from a single experiment performed in quadruplicate. Similar results were obtained in two independent experiments.

(D and E) Effect of (D) trametinib or (E) SCH772984 on pERK protein levels in *MEK*^{K57N} mutant and *MEK*^{WT} cell lines. Cells were treated with drug for 24 h and pERK levels determined by Western blot. MW (molecular weight markers) in Kilo Daltons.

(F) Time course Western blot analysis of the effect of ERK inhibitor (SCH772984, 500 nM) treatment on pERK and pCRAF protein levels in MEK^{K57N} mutant (KKU-M055) and *MEK*^{WT} G415 cells.

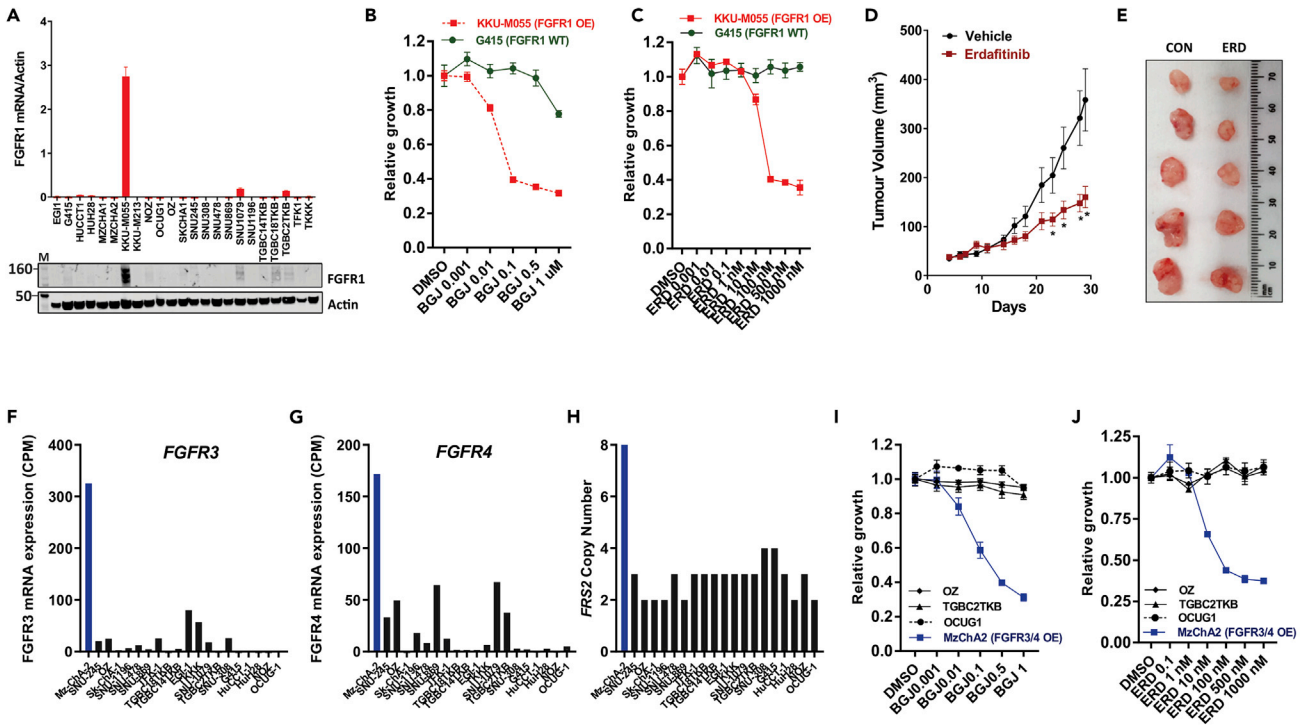

Figure 7. Characterization of FGFR Overexpressing BTC Cell Lines

(A) Basal (Top) mRNA and (Bottom) protein expression of *FGFR1* in the BTC cell line panel determined by qPCR and Western blot. M (molecular weight markers) in Kilo Daltons. Values shown in the top panel are mean + SEM from a single experiment performed in technical triplicate.

(B and C) Response of *FGFR1* overexpressing KKU-M055 cells and non-overexpressing G415 cells to increasing concentrations of (B) BGJ398 and (C) erdafitinib. Cells were treated for 72 h and cell growth determined by MTS assays. Values shown are mean ± SEM from a single experiment performed in quadruplicate. Similar results were obtained in three independent experiments.

(D and E) Response to KKU-M055 cells to erdafitinib *in vivo*. (D) Mice (n = 4 per group) were each injected with tumour cells in their right and left flanks and treated once daily via oral gavage with either erdafitinib (20 mg/kg) or vehicle (20% hydroxypropyl b cyclodextrin) for 18 consecutive days. Values shown in panel D are mean +/- SEM. (E) Representative images of resected tumours from mice treated with vehicle or erdafitanib.

(F and G) mRNA expression of (F) *FGFR3* and (G) *FGFR4* in the BTC cell line panel determined by RNA-seq. FGFR3/4 overexpressing Mz-Ch-A2 cells are shown in blue.

(H) *FRS2* DNA copy number in BTC cell lines.

(I and J) Response of FGFR3/4 overexpressing (blue) and non-overexpressing cell lines (black) to (I) BGJ398 and (J) erdafitinib *in vitro*. Cells were treated with drug for 72 h and cell growth determined by MTS assays. Values shown are mean +/- SEM from a representative experiment.

mutational signatures, and deletions and amplifications observed in primary tumors were also present in cell lines.

Cell lines exhibited a higher mutational burden to that reported in primary BTCs. This may be partly related to the lack of available normal genomic DNA for comparison. As a result, our somatic variant calling was dependent on comparisons to databases of known SNPs and germline mutations that may have overcalled the number of somatic mutations. Furthermore, cancer cell lines have undergone additional passages since the time of resection and hence have had the time to acquire additional mutations *in vitro*. Finally, it is possible that studies of primary BTC may under-call somatic variants, particularly tumors that have a high content of normal cells.

A major finding of the current study was the identification of sub classes of cell lines that differed primarily in the expression of genes involved in EMT, cell adhesion, differentiation, migration and developmental processes. Consistent with these transcriptional differences, the mesenchymal cluster was enriched for cell lines derived from metastatic gallbladder cancers, and morphological and histological analyses of the cell lines in this cluster revealed they were enriched for cell lines that had lost characteristics of epithelial differentiation. Importantly, we also observed similar differential expression of these epithelial/mesenchymal genes in tumor organoids derived from moderately and poorly differentiated tumors. The

advancement of 3D culture technology is now enabling the generation of increasing numbers of PDO model systems for use in translational research, and comparison of cell line and organoid platforms is of increasing interest. In this regard, it is noteworthy that our initial comparisons of these models, albeit using small numbers, suggest reasonable overlap. Finally, intersection of the epithelial and mesenchymal signatures identified in cell lines with RNA-seq data available through the TCGA revealed the existence of primary BTCs harboring both signatures, indicating these signatures are applicable to primary tumors. Indeed, primary BTCs that have lost expression of epithelial markers or that have gained expression of mesenchymal markers have been previously reported and associated with poorer outcome (Vaquero et al., 2017; Xu et al., 2017).

In comparison to our cell line analysis, prior gene expression profiling of primary BTCs identified four major groups of BTCs (Jusakul et al., 2017; Nakamura et al., 2015), including a group characterized by high expression of cytokines and immune checkpoint molecules. Gene expression profiling of intrahepatic cholangiocarcinomas also identified two major subclasses characterized by expression of proliferative and inflammatory genes, respectively. The contribution of stromal and inflammatory cells to the transcriptional signature of primary cancers likely contributes to these subtypes not being observed in cell lines and highlights an advantage of analyzing cell line models to reveal insights into biological differences among samples that may otherwise be masked by strong stromal signatures.

The genomic analysis of the BTC cell lines also revealed a number of potential actionable targets. In this regard, we tested a series of therapeutic targets established in other cancers for which we identified the corresponding endogenous genetic change in a BTC cell line. We identified the *R132C* hotspot mutation in *IDH1* in the SNU-1079 line, which had corresponding high levels of the onco-metabolite 2-HG. Notably, this cell line had the lowest mutational load among the cell lines and interestingly did not harbor mutations in any other established tumor suppressor genes or oncogenes, consistent with a potential epigenetic mechanism of tumor promotion in *IDH* mutant cancers (Farshidfar et al., 2017; Wang et al., 2013). The inhibitor of mutant *IDH1*, AGI-5198, inhibits colony formation of glioma cells transformed with mutant *IDH1* (Rohle et al., 2013); however, despite lowering of 2-HG levels, AGI-5198 or its clinically used derivative AG-120, had no effect on proliferation of SNU-1079 cells. Similarly, we observed that a PDO harboring an $IDH1^{R132L}$ mutation was also refractory to AG-120. These effects are consistent with pre-clinical studies in *IDH1* mutant chondrosarcoma (Saha et al., 2016), as well as recent clinical evidence in cholangiocarcinoma where objective responses were only observed in 6% of *IDH1* mutant patients treated with AG-120 (Lowery et al., 2017). Notably, the outcomes of the ClarIDHy phase III trial were recently reported in which *IDH1* mutant cholangiocarcinoma patients treated with AG-120 (ivosidenib) experienced a significant improvement in progression-free survival (2.7 months) compared with patients treated with placebo (1.4 months) (Abou-Alfa et al., 2019). Consistent with our findings in pre-clinical models, objective response were rare (2.4%), raising the possibility that inhibition of mutant IDH1 may elicit anti-tumour activity through non-cell autonomous mechanisms. Indeed, the oncometabolite 2-HG has been previously reported to promote angiogenesis (Seok et al., 2019) and suppress anti-tumour T cell immunity (Bunse et al., 2018).

On the other hand, we detected two cell lines harboring mutations and amplification of members of the ERBB receptor family, which demonstrated sensitivity to ERBB2-targeting agents. These findings are consistent with case reports and small clinical studies reporting clinical responses of BTCs to ERBB2 targeted agents (Hyman et al., 2018; Nam et al., 2016) and collectively support the fact that *ERBB2* amplification/mutations represent a promising therapeutic target in BTC.

An important finding of the current study is the identification of multiple mechanisms of ERK-MAPK pathway deregulation in BTC, whereby in addition to identifying mutations in *KRAS* in 36% of the cell lines, we identified *KRAS* amplifications in three lines, inactivating mutations in *BRAF* in two lines and a $MAP2K1^{K57T}$ mutation in one cell line. Notably, both inactivating *BRAF* mutations and the $MAP2K1^{K57T}$ mutation have been suggested to act as amplifiers of ERK-MAPK signaling and frequently co-exist with mutations in upstream components of the ERK-MAPK pathway (Gao et al., 2018; Yao et al., 2017). Indeed, detailed investigation of the cell lines harboring these mutations identified a co-existent activating *ERBB2* mutation in *BRAF* mutant (*I581L, N582T*) TGBC18TKB cells, an inactivating *RASA1* mutation in *BRAF*-mutant Sk-ChA-1 cells, and high levels of FGFR1 expression in $MAP2K1^{K57N}$ mutant KKU-M055 cells. An important implication of these findings is that tumors found to harbor low-activity "amplifier mutations" in the MAPK pathway in commonly used cancer gene panel sequencing tests should be further

interrogated for amplifications or overexpression of RTKs, as this may yield robust therapeutic targets. Proof of concept of this approach was our finding that *MAP2K1*^{K57N} mutant KKU-M055 cells express high levels of FGFR1 and are exquisitely sensitive to FGFR inhibition.

We also identified high levels of FGFR3 and FGFR4 expression in Mz-ChA-2 cells. Further interrogation of the FGFR signaling pathway in this line also revealed an amplification of *FRS2*, and Mz-Ch-A2 cells were highly sensitive to FGFR inhibition *in vitro*. This finding is consistent with observations in liposarcoma, where cell lines harboring *FRS2* amplifications have also been reported to be sensitive to FGFR inhibitors (Zhang et al., 2013). Importantly, gene fusions involving *FGFR2* occur in 7%–14% of intrahepatic cholangiocarcinomas (Helsten et al., 2016; Ross et al., 2014), and these tumors have been reported to be clinically responsive to FGFR inhibitors (Javle et al., 2018). Although we did not identify any cell lines harboring *FGFR2* fusions, our findings suggest that the subset of BTCs driven by aberrant FGFR signaling and amenable to FGFR inhibition extend beyond those harboring *FGFR2* fusions alone.

In summary, we characterized the exome, copy number, and transcriptome of a large panel of BTC cell lines and demonstrated that at the genomic level these cell line represent accurate models of primary disease. We also demonstrated that BTC cell lines can be separated into two major groups based on their transcriptional profiles, which is primarily driven by differential expression of genes involved in epithelial differentiation and EMT and which are also observed in both PDOs and primary tumors. We also identify a number of potential actionable drug targets for this disease (*ERBB2, FGFR1, and FGFR3/4*) and others that require additional investigation (*IDH1*) and provide a resource to facilitate the ongoing discovery and validation of potential therapeutic targets in BTC.

Limitations of the Study

An inherent limitation of the genomic analysis of historically established cell lines is the lack of normal genomic DNA for comparison, which may have resulted in miscalling of some genetic alterations. Cell lines also potentially acquire additional (epi-)genetic changes during passage, which may cause them to differ from primary tumors. Finally, the relatively small number of BTC cell lines available for genomic characterization is insufficient to capture all of genomic changes that drive BTC.

METHODS

All methods can be found in the accompanying Transparent Methods supplemental file.

SUPPLEMENTAL INFORMATION

Supplemental Information can be found online at https://doi.org/10.1016/j.isci.2019.10.044.

ACKNOWLEDGMENTS

This project was supported by the Victorian Cancer Agency (TRP13083), NHMRC Senior Research Fellowships to JMM (1046092) and OMS (1126119), and the Operational Infrastructure Support Program, Victorian Government, Australia. DL, LJ, and GI were supported by La Trobe University Australian Postgraduate Awards, and DL a scholarship from the Pancare Foundation, and GI a scholarship from the Hellenic Society of Medical Oncology. FC was supported by NHMRC Medical Postgraduate Scholarship (1017737), and YHY supported by a Fellowship from the ANZ Trustees Foundation (Brian Smith Endowment). We thank AGIOS Pharmaceuticals for measurement of 2-HG levels. The results shown here are in part based upon data generated by the TCGA Research Network: https://www.cancer.gov/tcga.

AUTHOR CONTRIBUTIONS

D.K.L., D.M, W.W., I.Y.L., C.M.S., D.S.W., G.I., L.J.J., C.M.R., T.M., Y.S., and J.M.M: conducted, analyzed, and interpreted experiments.

D.K.L., D.M, D.S.W., Y.Y., T.L., G.I., F.C., M.N., D.C, A.J.W., N.C.T., O.M.S and J.M.M: conceived, designed, interpreted experiments, and/or supervised parts of the study.

D.K.L., D.M, G.I., A.S.D., O.M.S, and J.M.M: contributed to the writing of the paper.

DECLARATION OF INTERESTS

The authors declare no competing interests.

Received: July 5, 2019
Revised: September 21, 2019
Accepted: October 22, 2019
Published: November 22, 2019

REFERENCES

Abou-Alfa, G.K., Maraculla, T.M., Javle, M., et al., (2019) and ClarIDHy: A global, phase 3, randomized, double-blind study of ivosidenib (IVO) vs placebo in patients with advanced cholangiocarcinoma (CC) with an isocitrate dehydrogenase 1 (IDH1) mutation. Presented at: 2019 ESMO Congress; September 27 to October 1, 2019; Barcelona, Spain. Abstract LBA10_PR. https://oncologypro.esmo.org/Meeting-Resources/ESMO-2019-Congress/ClarIDHy-A-global-phase-3-randomized-double-blind-study-of-ivosidenib-IVO-vs-placebo-in-patients-with-advanced-cholangiocarcinoma-CC-with-an-isocitrate-dehydrogenase-1-IDH1-mutation.

Alexandrov, L.B., Nik-Zainal, S., Wedge, D.C., Aparicio, S.A., Behjati, S., Biankin, A.V., Bignell, G.R., Bolli, N., Borg, A., Borresen-Dale, A.L., et al. (2013). Signatures of mutational processes in human cancer. Nature *500*, 415–421.

Arai, Y., Totoki, Y., Hosoda, F., Shirota, T., Hama, N., Nakamura, H., Ojima, H., Furuta, K., Shimada, K., Okusaka, T., et al. (2014). Fibroblast growth factor receptor 2 tyrosine kinase fusions define a unique molecular subtype of cholangiocarcinoma. Hepatology *59*, 1427–1434.

Borger, D.R., Tanabe, K.K., Fan, K.C., Lopez, H.U., Fantin, V.R., Straley, K.S., Schenkein, D.P., Hezel, A.F., Ancukiewicz, M., Liebman, H.M., et al. (2012). Frequent mutation of isocitrate dehydrogenase (IDH)1 and IDH2 in cholangiocarcinoma identified through broad-based tumor genotyping. Oncologist *17*, 72–79.

Bunse, L., Pusch, S., Bunse, T., Sahm, F., Sanghvi, K., Friedrich, M., Alansary, D., Sonner, J.K., Green, E., Deumelandt, K., et al. (2018). Suppression of antitumor T cell immunity by the oncometabolite (R)-2-hydroxyglutarate. Nat. Med. *24*, 1192–1203.

Chan-On, W., Nairismagi, M.L., Ong, C.K., Lim, W.K., Dima, S., Pairojkul, C., Lim, K.H., McPherson, J.R., Cutcutache, I., Heng, H.L., et al. (2013). Exome sequencing identifies distinct mutational patterns in liver fluke-related and non-infection-related bile duct cancers. Nat. Genet. *45*, 1474–1478.

Charbel, H., and Al-Kawas, F.H. (2011). Cholangiocarcinoma: epidemiology, risk factors, pathogenesis, and diagnosis. Curr. Gastroenterol. Rep. *13*, 182–187.

Dougherty, M.K., Muller, J., Ritt, D.A., Zhou, M., Zhou, X.Z., Copeland, T.D., Conrads, T.P., Veenstra, T.D., Lu, K.P., and Morrison, D.K. (2005). Regulation of Raf-1 by direct feedback phosphorylation. Mol. Cell *17*, 215–224.

Farshidfar, F., Zheng, S., Gingras, M.C., Newton, Y., Shih, J., Robertson, A.G., Hinoue, T., Hoadley, K.A., Gibb, E.A., Roszik, J., et al. (2017). Integrative genomic analysis of cholangiocarcinoma identifies distinct IDH-mutant molecular profiles. Cell Rep. *19*, 2878–2880.

Gao, Y., Chang, M.T., McKay, D., Na, N., Zhou, B., Yaeger, R., Torres, N.M., Muniz, K., Drosten, M., Barbacid, M., et al. (2018). Allele-specific mechanisms of activation of MEK1 mutants determine their properties. Cancer Discov. *8*, 648–661.

Helsten, T., Elkin, S., Arthur, E., Tomson, B.N., Carter, J., and Kurzrock, R. (2016). The FGFR landscape in cancer: analysis of 4,853 tumors by next-generation sequencing. Clin. Cancer Res. *22*, 259–267.

Homma, S., Hasumura, S., Nagamori, S., and Kameda, H. (1988). Establishment and characterization of a human gall bladder carcinoma cell line NOZ. Hum. Cell *1*, 95–97.

Homma, S., Nagamori, S., Fujise, K., Yamazaki, K., Hasumura, S., Sujino, H., Matsuura, T., Shimizu, K., Kameda, H., and Takaki, K. (1987). Human bile duct carcinoma cell line producing abundant mucin in vitro. Gastroenterol. Jpn. *22*, 474–479.

Hyman, D.M., Piha-Paul, S.A., Won, H., Rodon, J., Saura, C., Shapiro, G.I., Juric, D., Quinn, D.I., Moreno, V., Doger, B., et al. (2018). HER kinase inhibition in patients with HER2- and HER3-mutant cancers. Nature *554*, 189–194.

Ishii, Y., Sigel, C., Lowery, M.A., Goyal, L., Gliser, C., Jiang, L., Pandya, S., Wu, B., Choe, S., and Deshpande, V. (2018). Abstract A071: AG-120 (ivosidenib), a first-in-class mutant IDH1 inhibitor, promotes morphologic changes and upregulates liver-specific genes in IDH1 mutant cholangiocarcinoma. Mol. Cancer Ther. *17*, A071.

Javle, M., Lowery, M., Shroff, R.T., Weiss, K.H., Springfeld, C., Borad, M.J., Ramanathan, R.K., Goyal, L., Sadeghi, S., Macarulla, T., et al. (2018). Phase II study of BGJ398 in patients with FGFR-altered advanced cholangiocarcinoma. J. Clin. Oncol. *36*, 276–282.

Jusakul, A., Cutcutache, I., Yong, C.H., Lim, J.Q., Huang, M.N., Padmanabhan, N., Nellore, V., Kongpetch, S., Ng, A.W.T., Ng, L.M., et al. (2017). Whole-genome and epigenomic landscapes of etiologically distinct subtypes of cholangiocarcinoma. Cancer Discov. *7*, 1116–1135.

Knuth, A., Gabbert, H., Dippold, W., Klein, O., Sachsse, W., Bitter-Suermann, D., Prellwitz, W., and Meyer zum Buschenfelde, K.H. (1985). Biliary adenocarcinoma. Characterisation of three new human tumor cell lines. J. Hepatol. *1*, 579–596.

Koo, B.K., Spit, M., Jordens, I., Low, T.Y., Stange, D.E., van de Wetering, M., van Es, J.H., Mohammed, S., Heck, A.J., Maurice, M.M., et al. (2012). Tumour suppressor RNF43 is a stem-cell E3 ligase that induces endocytosis of Wnt receptors. Nature *488*, 665–669.

Koyama, S., Yoshioka, T., Mizushima, A., Kawakita, I., Yamagata, S., Fukutomi, H., Sakita, T., Kondo, I., and Kikuchi, M. (1980). Establishment of a cell line (G-415) from a human gallbladder carcinoma. Gan *71*, 574–575.

Ku, J.L., Yoon, K.A., Kim, I.J., Kim, W.H., Jang, J.Y., Suh, K.S., Kim, S.W., Park, Y.H., Hwang, J.H., Yoon, Y.B., et al. (2002). Establishment and characterisation of six human biliary tract cancer cell lines. Br. J. Cancer *87*, 187–193.

Kusaka, Y., Tokiwa, T., and Sato, J. (1988). Establishment and characterization of a cell line from a human cholangiocellular carcinoma. Res. Exp. Med. (Berl) *188*, 367–375.

Lapinski, P.E., Bauler, T.J., Brown, E.J., Hughes, E.D., Saunders, T.L., and King, P.D. (2007). Generation of mice with a conditional allele of the p120 Ras GTPase-activating protein. Genesis *45*, 762–767.

Li, M., Zhang, Z., Li, X., Ye, J., Wu, X., Tan, Z., Liu, C., Shen, B., Wang, X.A., Wu, W., et al. (2014). Whole-exome and targeted gene sequencing of gallbladder carcinoma identifies recurrent mutations in the ErbB pathway. Nat. Genet. *46*, 872–876.

Lowery, M.A., Abou-Alfa, G.K., Burris, H.A., Janku, F., Shroff, R.T., Cleary, J.M., Saba Azad, N., Goyal, L., Maher, E.A., Gore, L., et al. (2017). Phase I study of AG-120, an IDH1 mutant enzyme inhibitor: results from the cholangiocarcinoma dose escalation and expansion cohorts. J. Clin. Oncol. *35*, 4015.

Marcano-Bonilla, L., Mohamed, E.A., Mounajjed, T., and Roberts, L.R. (2016). Biliary tract cancers: epidemiology, molecular pathogenesis and genetic risk associations. Chin. Clin. Oncol. *5*, 61.

Miyagiwa, M., Ichida, T., Tokiwa, T., Sato, J., and Sasaki, H. (1989). A new human cholangiocellular carcinoma cell line (HuCC-T1) producing carbohydrate antigen 19/9 in serum-free medium. In Vitro Cell Dev. Biol. *25*, 503–510.

Molenaar, R.J., Maciejewski, J.P., Wilmink, J.W., and van Noorden, C.J.F. (2018). Wild-type and mutated IDH1/2 enzymes and therapy responses. Oncogene *37*, 1949–1960.

Nakamura, H., Arai, Y., Totoki, Y., Shirota, T., Elzawahry, A., Kato, M., Hama, N., Hosoda, F., Urushidate, T., Ohashi, S., et al. (2015). Genomic spectra of biliary tract cancer. Nat. Genet. *47*, 1003–1010.

Nam, A.R., Kim, J.W., Cha, Y., Ha, H., Park, J.E., Bang, J.H., Jin, M.H., Lee, K.H., Kim, T.Y., Han, S.W., et al. (2016). Therapeutic implication of HER2 in advanced biliary tract cancer. Oncotarget *7*, 58007–58021.

Obchoei, S., Weakley, S.M., Wongkham, S., Wongkham, C., Sawanyawisuth, K., Yao, Q., and Chen, C. (2011). Cyclophilin A enhances cell proliferation and tumor growth of liver fluke-associated cholangiocarcinoma. Mol. Cancer *10*, 102.

Ong, C.K., Subimerb, C., Pairojkul, C., Wongkham, S., Cutcutache, I., Yu, W., McPherson, J.R., Allen, G.E., Ng, C.C., Wong, B.H., et al. (2012). Exome sequencing of liver fluke-associated cholangiocarcinoma. Nat. Genet. *44*, 690–693.

Rohle, D., Popovici-Muller, J., Palaskas, N., Turcan, S., Grommes, C., Campos, C., Tsoi, J., Clark, O., Oldrini, B., Komisopoulou, E., et al. (2013). An inhibitor of mutant IDH1 delays growth and promotes differentiation of glioma cells. Science *340*, 626–630.

Ross, J.S., Wang, K., Gay, L., Al-Rohil, R., Rand, J.V., Jones, D.M., Lee, H.J., Sheehan, C.E., Otto, G.A., Palmer, G., et al. (2014). New routes to targeted therapy of intrahepatic cholangiocarcinomas revealed by next-generation sequencing. Oncologist *19*, 235–242.

Saha, S.K., Gordan, J.D., Kleinstiver, B.P., Vu, P., Najem, M.S., Yeo, J.C., Shi, L., Kato, Y., Levin, R.S., Webber, J.T., et al. (2016). Isocitrate dehydrogenase mutations confer dasatinib hypersensitivity and SRC dependence in intrahepatic cholangiocarcinoma. Cancer Discov. *6*, 727–739.

Saha, S.K., Parachoniak, C.A., and Bardeesy, N. (2014). IDH mutations in liver cell plasticity and biliary cancer. Cell Cycle *13*, 3176–3182.

Saito, Y., Muramatsu, T., Kanai, Y., Ojima, H., Sukeda, A., Hiraoka, N., Arai, E., Sugiyama, Y., Matsuzaki, J., Uchida, R., et al. (2019). Establishment of patient-derived organoids and drug screening for biliary tract carcinoma. Cell Rep. *27*, 1265–1276.e64.

Seok, J., Yoon, S.H., Lee, S.H., Jung, J.H., and Lee, Y.M. (2019). The oncometabolite d2hydroxyglutarate induces angiogenic activity through the vascular endothelial growth factor receptor 2 signaling pathway. Int. J. Oncol. *54*, 753–763.

Shoda, J., Ishige, K., Sugiyama, H., and Kawamoto, T. (2012). Biliary tract carcinoma: clinical perspectives on molecular targeting strategies for therapeutic options. J. Hepatobiliary Pancreat. Sci. *19*, 342–353.

Tepsiri, N., Chaturat, L., Sripa, B., Namwat, W., Wongkham, S., Bhudhisawasdi, V., and Tassaneeyakul, W. (2005). Drug sensitivity and drug resistance profiles of human intrahepatic cholangiocarcinoma cell lines. World J. Gastroenterol. *11*, 2748–2753.

Turner, N., and Grose, R. (2010). Fibroblast growth factor signalling: from development to cancer. Nat. Rev. Cancer *10*, 116–129.

Valle, J., Wasan, H., Palmer, D.H., Cunningham, D., Anthoney, A., Maraveyas, A., Madhusudan, S., Iveson, T., Hughes, S., Pereira, S.P., et al. (2010). Cisplatin plus gemcitabine versus gemcitabine for biliary tract cancer. N. Engl. J. Med. *362*, 1273–1281.

Vaquero, J., Guedj, N., Claperon, A., Nguyen Ho-Bouldoires, T.H., Paradis, V., and Fouassier, L. (2017). Epithelial-mesenchymal transition in cholangiocarcinoma: from clinical evidence to regulatory networks. J. Hepatol. *66*, 424–441.

Wang, P., Dong, Q., Zhang, C., Kuan, P.F., Liu, Y., Jeck, W.R., Andersen, J.B., Jiang, W., Savich, G.L., Tan, T.X., et al. (2013). Mutations in isocitrate dehydrogenase 1 and 2 occur frequently in intrahepatic cholangiocarcinomas and share hypermethylation targets with glioblastomas. Oncogene *32*, 3091–3100.

Ward, P.S., Patel, J., Wise, D.R., Abdel-Wahab, O., Bennett, B.D., Coller, H.A., Cross, J.R., Fantin, V.R., Hedvat, C.V., Perl, A.E., et al. (2010). The common feature of leukemia-associated IDH1 and IDH2 mutations is a neomorphic enzyme activity converting alpha-ketoglutarate to 2-hydroxyglutarate. Cancer Cell *17*, 225–234.

Xu, S., Zhan, M., and Wang, J. (2017). Epithelial-to-mesenchymal transition in gallbladder cancer: from clinical evidence to cellular regulatory networks. Cell Death Discov. *3*, 17069.

Yamada, N., Chung, Y., Ohtani, H., Ikeda, T., Onoda, N., Sawada, T., Nishiguchi, Y., Hasuma, T., and Sowa, M. (1997). Establishment and characterization of a new human gallbladder carcinoma cell line (OCUG-1) producing TA-4. Int. J. Oncol. *10*, 1251–1255.

Yao, Z., Yaeger, R., Rodrik-Outmezguine, V.S., Tao, A., Torres, N.M., Chang, M.T., Drosten, M., Zhao, H., Cecchi, F., Hembrough, T., et al. (2017). Tumours with class 3 BRAF mutants are sensitive to the inhibition of activated RAS. Nature *548*, 234–238.

Zhang, K., Chu, K., Wu, X., Gao, H., Wang, J., Yuan, Y.C., Loera, S., Ho, K., Wang, Y., Chow, W., et al. (2013). Amplification of FRS2 and activation of FGFR/FRS2 signaling pathway in high-grade liposarcoma. Cancer Res. *73*, 1298–1307.

ISCI, Volume *21*

Supplemental Information

Genomic Profiling of Biliary Tract Cancer Cell Lines Reveals Molecular Subtypes and Actionable Drug Targets

David K. Lau, Dmitri Mouradov, Wiphawan Wasenang, Ian Y. Luk, Cameron M. Scott, David S. Williams, Yvonne H. Yeung, Temduang Limpaiboon, George F. Iatropoulos, Laura J. Jenkins, Camilla M. Reehorst, Fiona Chionh, Mehrdad Nikfarjam, Daniel Croagh, Amardeep S. Dhillon, Andrew J. Weickhardt, Toshihide Muramatsu, Yoshimasa Saito, Niall C. Tebbutt, Oliver M. Sieber, and John M. Mariadason

Figure S1

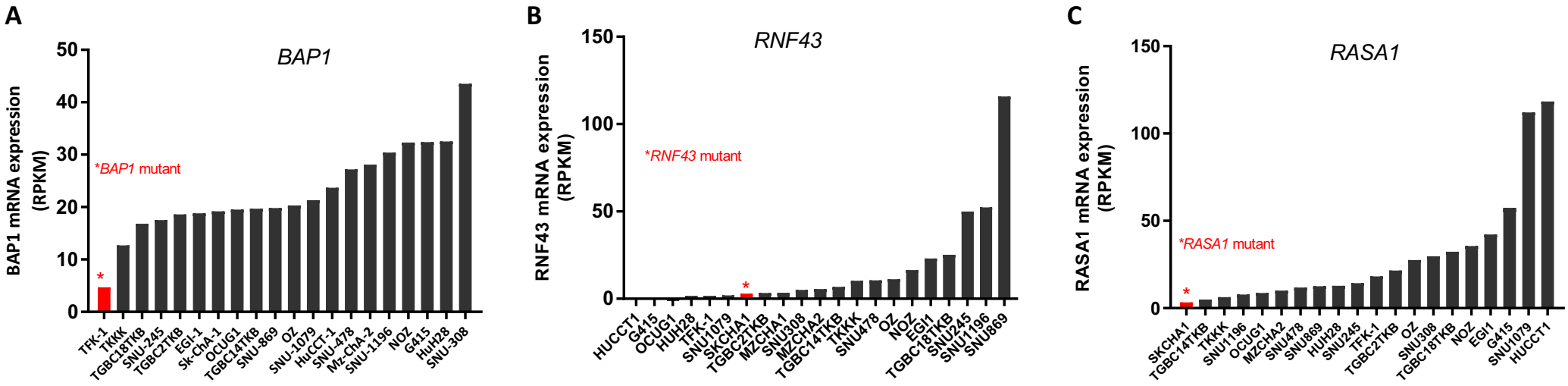

Figure S1. mRNA expression of genes harboring inactivating mutations, Related to Figure 2. mRNA expression of (A) BAP1 (B) RNF43 and (C) RASA1 in BTC lines determined by RNA-seq.

Figure S2

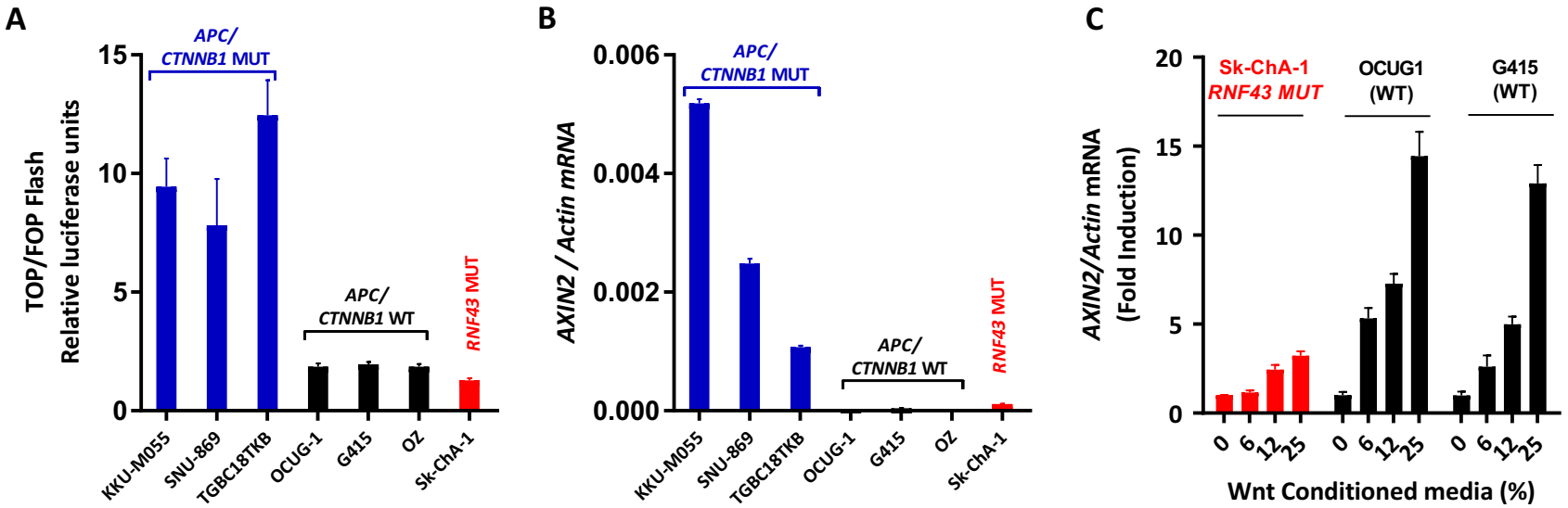

Figure S2. Validation of altered Wnt signaling in BTC cell lines, Related to Figure 2. (**A**) Wnt reporter activity in BTC cell lines which are mutant or wild type for *APC*, *CTNNB1* or *RNF43* determined by the ration of TOPFLASH/FOPFLASH (TOP/FOP) luciferase reporter assay. Values shown are mean + SEM from a representative experiment performed in quadruplicate. (**B**) Basal mRNA expression of the Wnt target gene *AXIN2* in BTC cell lines determined by qPCR. Values shown are mean + SEM from a representative experiment performed in technical triplicate. (**C**) Effect of Wnt3a conditioned medium of mRNA expression of *AXIN2* in BTC cell lines. Cells were treated with increasing concentrations of Wnt3a conditioned medium for 24h and *AXIN2* mRNA expression determined by qPCR. Values shown are mean + SEM from a representative experiment performed in technical quadruplicate.

Figure S3

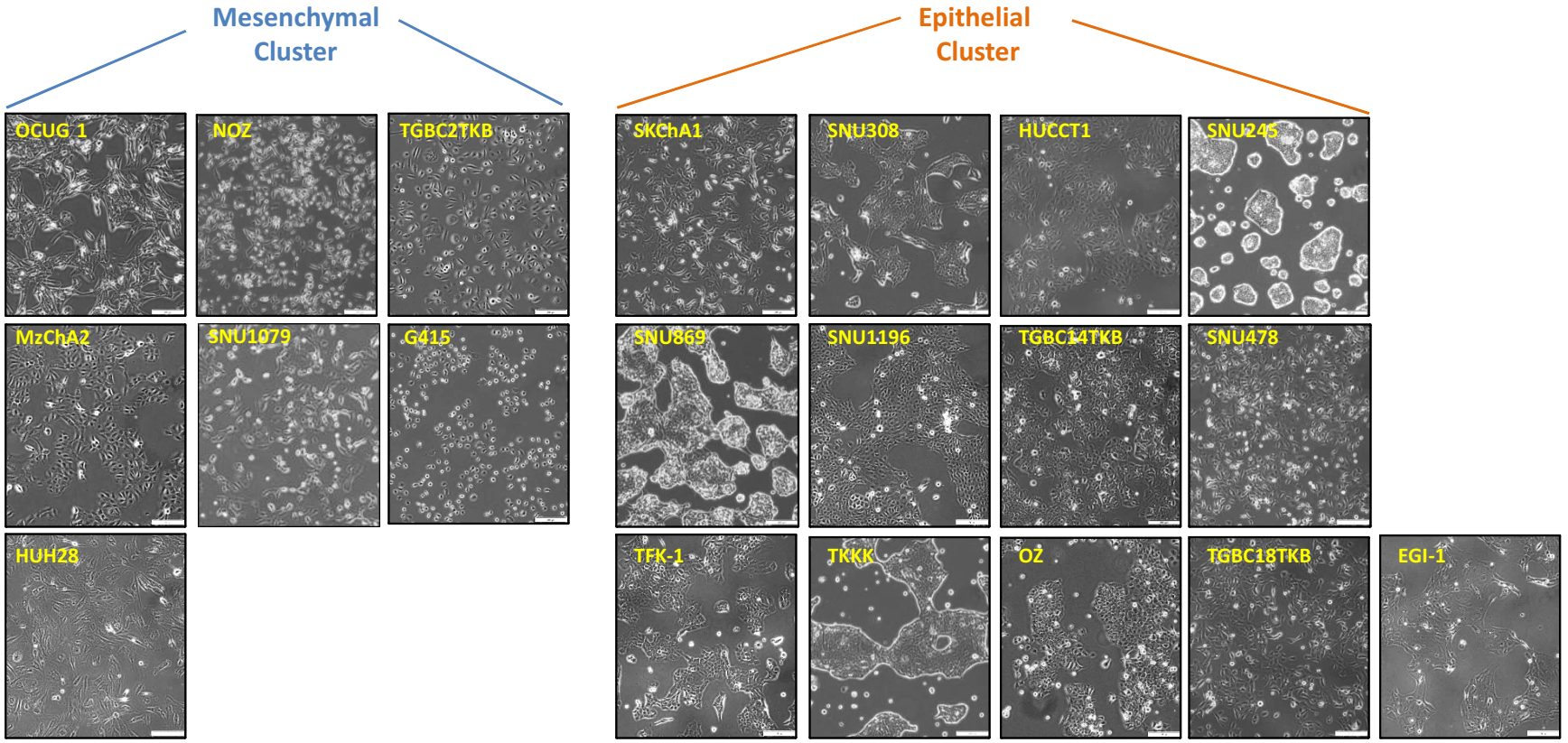

Figure S3. Morphology of BTC cell lines from the mesenchymal and epithelial clusters when grown in 2D cell culture, Related to Figure 4. Cell lines in the exponentially growing phase were imaged by light microscopy.

Figure S4

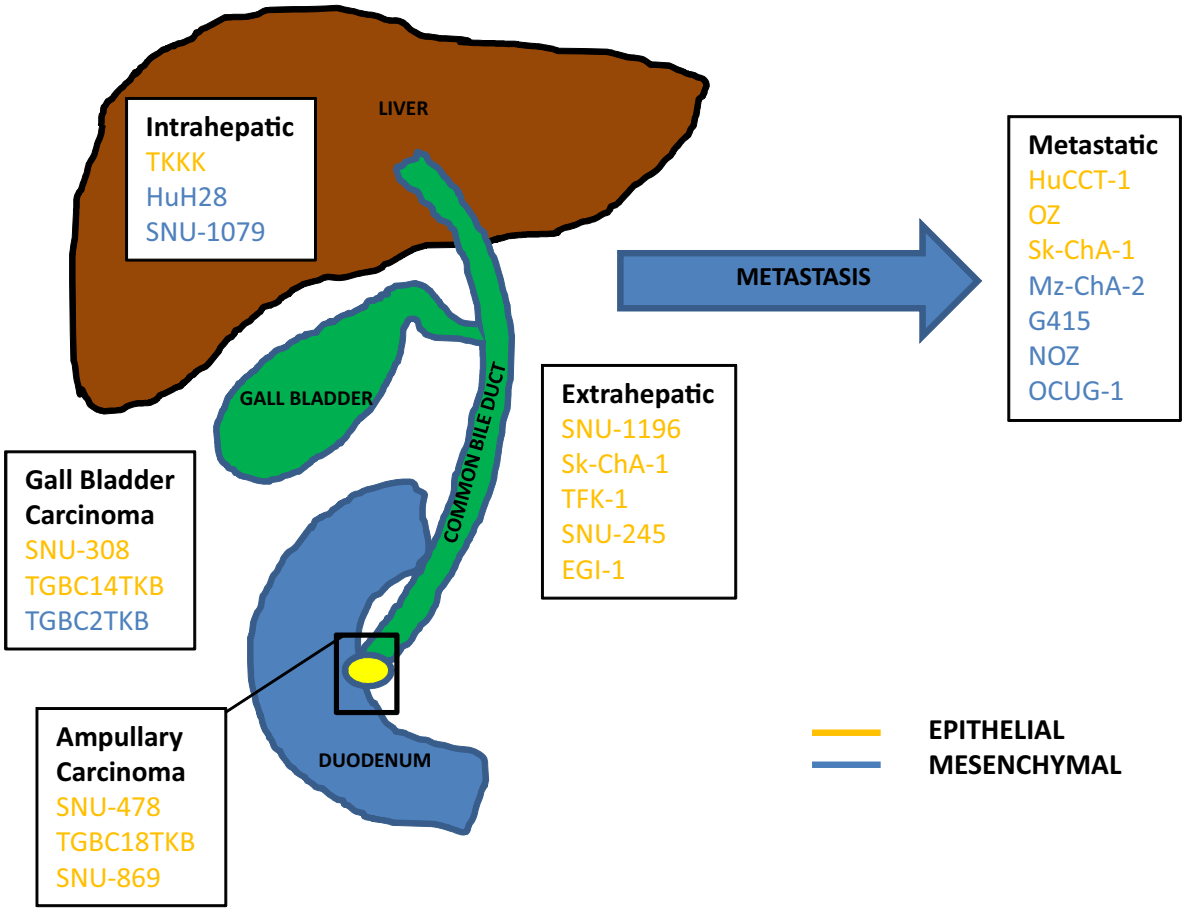

Figure S4. Summary of anatomical location and molecular subtype of BTC cell lines, Related to Figure 4. Cell lines were classified as epithelial or mesenchymal based on their basal gene expression profile which was assessed by RNA-seq analysis.

Figure S5

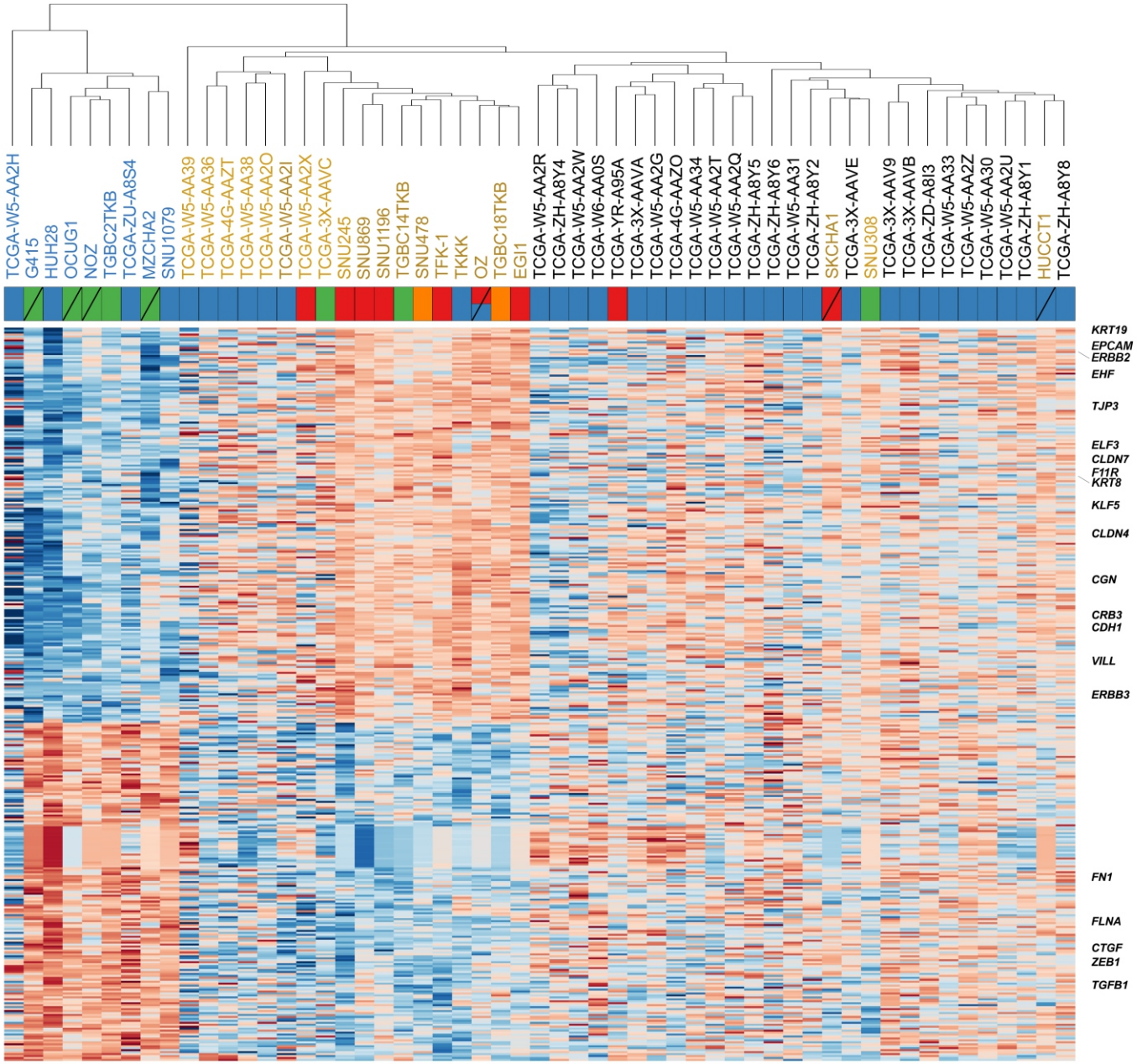

Figure S5. Identification or primary BTCs harboring the mesenchymal (blue text) and epithelial (orange text) signatures identified in BTC cell lines, Related to Figure 4. 35 primary BTCs for which RNA-seq data was available were clustered along with the 20 BTC cell lines based on the expression of the 411 genes differentially expressed between the epithelial and mesenchymal BTC cell line clusters. Two primary BTCs (TCGA-W5-AA2H and TCGA-ZU-A824) clustered with the cell lines harboring the mesenchymal signature, and 8 primary BTCs (TCGA-W5-AA39, TCGA-W5-AA36, TCGA-4G-AAZT, TCGA-W5-AA38, TCGA-W5-AA2O, TCGA-W5-AA2I, TCGA-W5-AA2X and TCGA-3X-AACV) clustered with the BTC cell lines harboring the epithelial signature. Data obtained in part from the TCGA Research Network: https://www.cancer.gov/tcga.

Figure S6

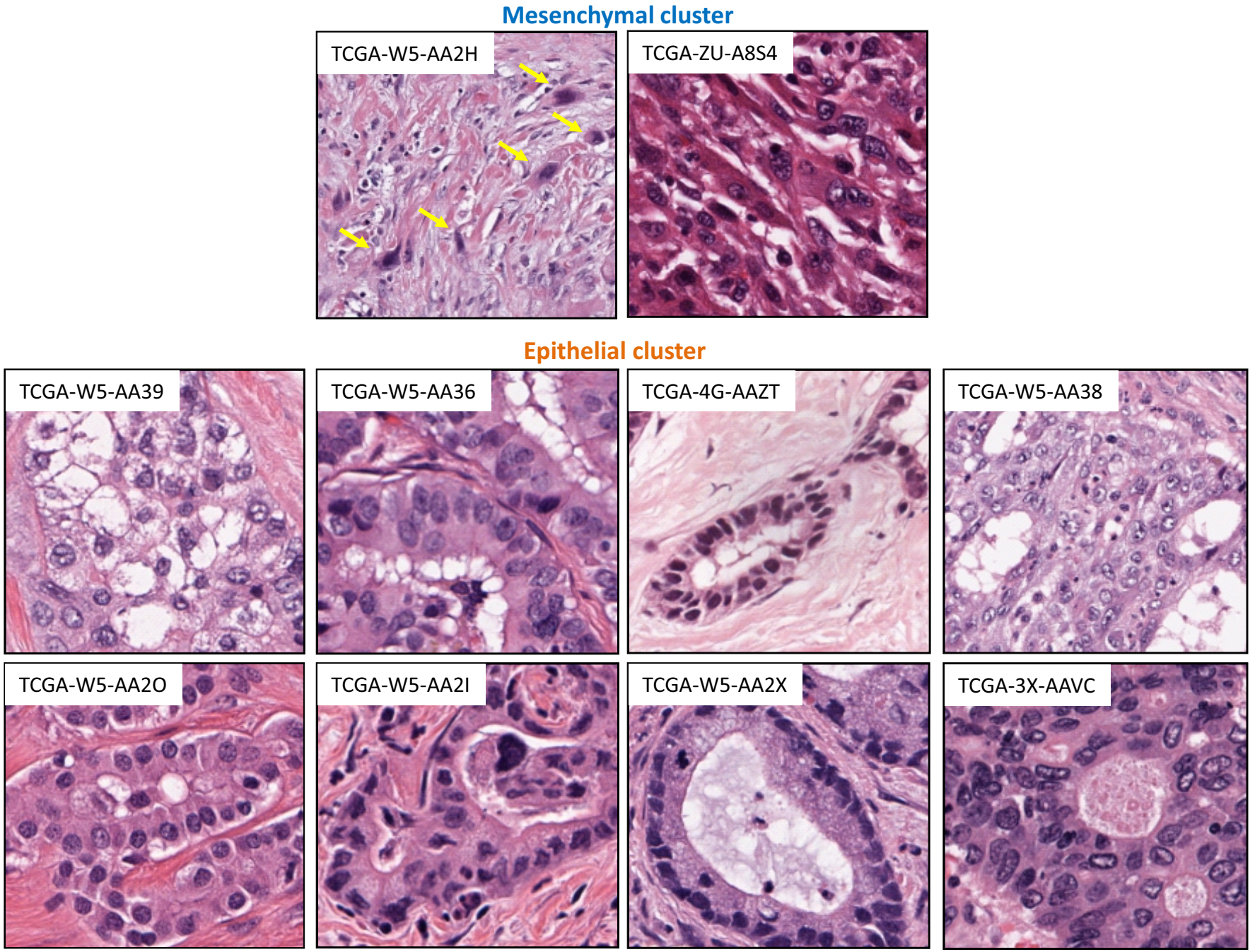

Figure S6. Cellular morphology of primary tumours clustered among the cell lines harbouring the mesenchymal or epithelial signature, Related to Figure 4. Images obtained from the TCGA Research Network: https://www.cancer.gov/tcga.

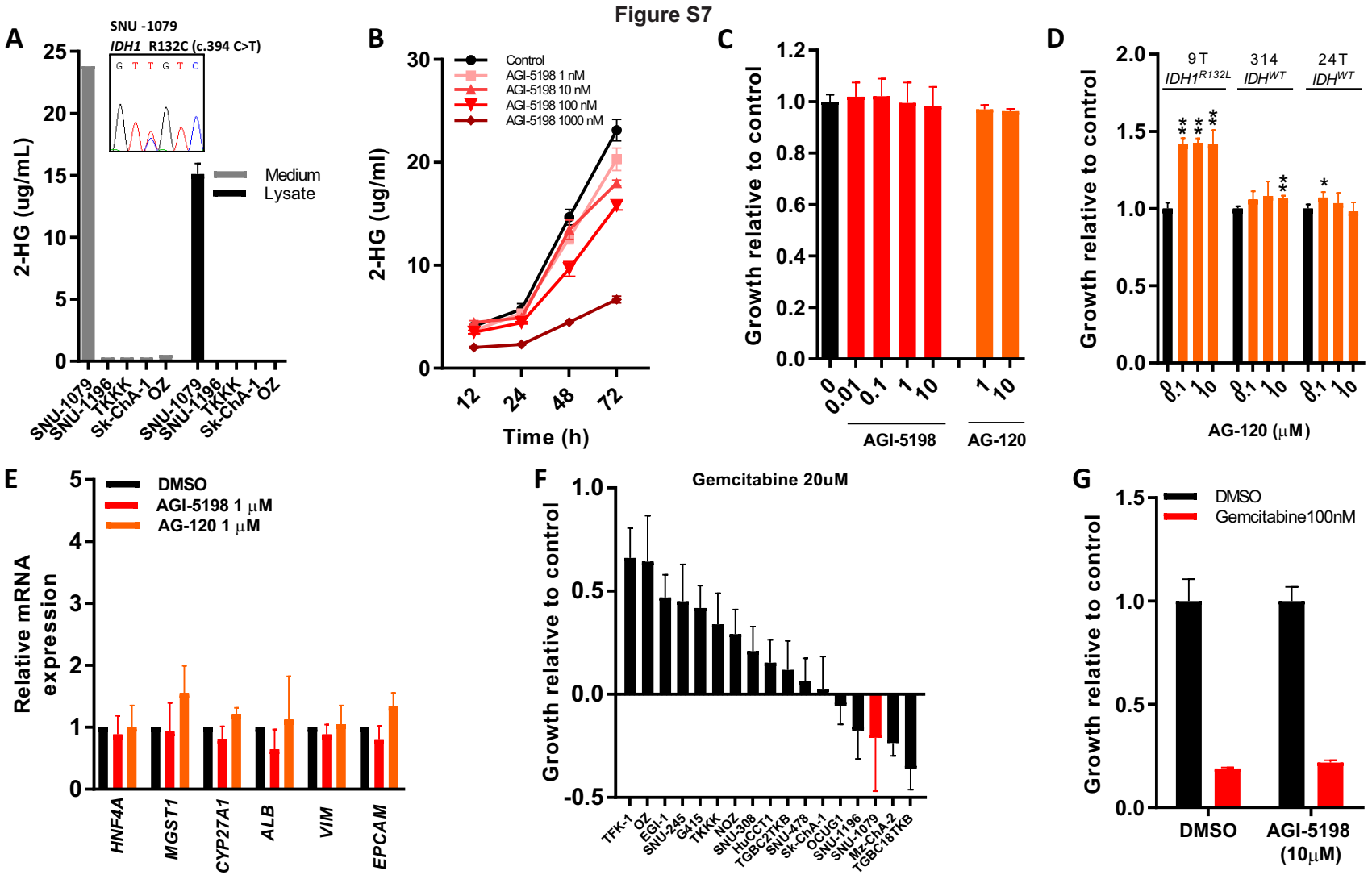

Figure S7. Characterization of *IDH1*^{R132C} mutant SNU-1079 cells, Related to Figure 2. (**A**) Levels of 2-HG in the culture medium or cell lysates in *IDH*^{R132C} (SNU-1079) or *IDH*^{WT} (SNU-1196, TKKK, Sk-Ch-A1, OZ) cell lines. Values shown are mean + SD from a representative experiment performed in duplicate. Inset: Sanger sequencing chromatogram of *IDH1 R132C* mutation in SNU-1079 cells. (**B**) SNU-1079 cells were treated with increasing concentrations of the mutant IDH1 inhibitor AGI-5198 for up to 72h and 2-HG levels determined in the culture medium. Values shown are mean +/- SEM of a representative experiment performed in technical triplicate. (**C**) Effect of AGI-5198 and AG-120 on proliferation of SNU-1079 cells. Cells were treated with AGI-5198 or AG-120 for 72h and cell proliferation determined using the MTS assay. Values shown are mean + SEM of n=3 independent experiments. (**D**) Effect of AG-120 on proliferation of *IDH1*^{R132L} or *IDH*^{WT} biliary cancer organoids. Values shown are mean+SD of a representative experiment performed in quadruplicate. Similar results were obtained in an independent experiment. (**E**) Effect of AGI-5189 and AG-120 on expression of markers of hepatocyte differentiation and EMT. SNU-1079 cells were treated with AGI-5198 or AG-120 for 72h and changes in gene expression determined by qPCR. Values shown are mean + SEM of a representative experiment performed in triplicate. (**F**) Relative sensitivity of BTC cell lines to gemcitabine. Cells were treated with DMSO or gemcitabine (20 uM) for 72h and cell viability determined by MTS assay. Values shown are mean + SD of n=2 independent experiments. (**G**) Effect of combination treatment with AGI-5198 and gemcitabine on proliferation of IDH mutant SNU-1079 cells. Cells were treated with drug combinations for 72h and cell proliferation determined by MTS assay. Values shown are mean + SD from a representative experiment performed in technical quadruplicate.

Table S1. Biliary tract cancer cell lines, source and origin, Related to Figure 1. HSRRB-Japan Health Sciences Foundation; Zurich University (Prof. A Knuth); KCLB-Korean Cell Line Bank; RIKEN Bioresources Centre, Japan.

Cell line	Gender, Age	Differentiation grade of primary	Anatomical location of primary tumour	Primary/ Metastatic	Liver Fluke	Source	Ref
HuH28	Female, 37Y	Undiff	Intrahepatic	Primary	No	HSRRB	(1)
SNU-1079	Male, Unk	Mod Diff	Intrahepatic	Primary	No	KCLB	(2)
TKKK	Male, Unk	Unk	Intrahepatic	Primary	No	RIKEN	N/A
KKU-M055	Male, 56Y	Poorly Diff	Intrahepatic	Primary	Yes	KKU	(3)
KKU-M213	Male, 58Y	Adenosquamous	Intrahepatic	Primary	Yes	KKU	(4)
HuCCT1	Male, 56Y	Mod Diff	Intrahepatic	Metastatic (Ascites)	No	RIKEN	(5)
OZ	Male, 71Y	Well Diff and Poorly Diff	Extra/Intrahepatic	Metastatic (Ascites)	No	HSRRB	(6)
SNU-1196	Unk, Unk	Mod Diff	Extrahepatic	Primary	No	KCLB	(2)
Sk-ChA-1	Female, 47Y	Undiff	Extrahepatic	Metastatic (Ascites)	No	Zurich Uni.	(7)
TFK-1	Male, 63Y	Mod Diff	Extrahepatic	Primary	No	DSMZ	(8)
SNU-245	Unk, Unk	Well Diff	Extrahepatic	Primary	No	KCLB	(2)
EGI-1	Male, 52Y	Poorly Diff	Extrahepatic	Primary	No	DSMZ	(9)
SNU-308	Unk, Unk	Well-Mod Diff	Gallbladder	Primary	No	KCLB	(2)
TGBC14TKB	Female, Unk	Undiff (Anaplastic)	Gallbladder	Primary	No	RIKEN	(10)
TGBC2TKB	Female, Unk	Well/Poorly Diff	Gallbladder	Primary	No	RIKEN	(10)
Mz-ChA-2	Female, 63Y	Mod Diff	Gallbladder	Metastatic (liver)	No	Zurich Uni.	(7)
G415	Male, 68Y	Undiff	Gallbladder	Metastatic (Ascites)	No	RIKEN	(11)
NOZ	Female, 48Y	Mod Diff	Gallbladder	Metastatic (Ascites	No	HSRRB	(12)
OCUG-1	Male, 43Y	Poorly Diff	Gallbladder	Metastatic (Ascites)	No	HSRRB	(13)
SNU-478	Unk, Unk	Poorly Diff	Ampullary	Primary	No	KCLB	(2)
TGBC18TKB	Female, 79Y	Unk	Ampullary	Primary	No	RIKEN	N/A
SNU-869	Unk, Unk	Well Diff	Ampullary	Primary	No	KCLB	(2)

1. Kusaka Y, Tokiwa T, Sato J. Establishment and characterization of a cell line from a human cholangiocellular carcinoma. Res Exp Med (Berl) **1988**;188:367-75
2. Ku JL, Yoon KA, Kim IJ, Kim WH, Jang JY, Suh KS*, et al.* Establishment and characterisation of six human biliary tract cancer cell lines. Br J Cancer **2002**;87:187-93
3. Tepsiri N, Chaturat L, Sripa B, Namwat W, Wongkham S, Bhudhisawasdi V*, et al.* Drug sensitivity and drug resistance profiles of human intrahepatic cholangiocarcinoma cell lines. World J Gastroenterol **2005**;11:2748-53

4. Obchoei S, Weakley SM, Wongkham S, Wongkham C, Sawanyawisuth K, Yao Q*, et al.* Cyclophilin A enhances cell proliferation and tumor growth of liver fluke-associated cholangiocarcinoma. Molecular cancer **2011**;10:102
5. Miyagiwa M, Ichida T, Tokiwa T, Sato J, Sasaki H. A new human cholangiocellular carcinoma cell line (HuCC-T1) producing carbohydrate antigen 19/9 in serum-free medium. In Vitro Cell Dev Biol **1989**;25:503-10
6. Homma S, Nagamori S, Fujise K, Yamazaki K, Hasumura S, Sujino H*, et al.* Human bile duct carcinoma cell line producing abundant mucin in vitro. Gastroenterol Jpn **1987**;22:474-9
7. Knuth A, Gabbert H, Dippold W, Klein O, Sachsse W, Bitter-Suermann D*, et al.* Biliary adenocarcinoma. Characterisation of three new human tumor cell lines. Journal of hepatology **1985**;1:579-96
8. Saijyo S, Kudo T, Suzuki M, Katayose Y, Shinoda M, Muto T*, et al.* Establishment of a new extrahepatic bile duct carcinoma cell line, TFK-1. Tohoku J Exp Med **1995**;177:61-71
9. Zach S, Birgin E, Rückert F. Primary Cholangiocellular Carcinoma Cell Lines. J Stem Cell Res Transplant **2015**;2:1013
10. Ghosh M, Koike N, Yanagimoto G, Tsunoda S, Kaul S, Hirano T*, et al.* Establishment and characterization of unique human gallbladder cancer cell lines. Int J Oncol **2004**;24:1189-96
11. Koyama S, Yoshioka T, Mizushima A, Kawakita I, Yamagata S, Fukutomi H*, et al.* Establishment of a cell line (G-415) from a human gallbladder carcinoma. Gan **1980**;71:574-5
12. Homma S, Hasumura S, Nagamori S, Kameda H. [Establishment and characterization of a human gall bladder carcinoma cell line NOZ]. Hum Cell **1988**;1:95-7
13. Yamada N, Chung Y, Ohtani H, Ikeda T, Onoda N, Sawada T*, et al.* Establishment and characterization of a new human gallbladder carcinoma cell line (OCUG-1) producing TA-4. Int J Oncol **1997**;10:1251-5

Table S2. Mutated genes in 22 BTC cell lines, Related to Figure 1. Table is provided as a separate excel file.

Table S3. Significantly Amplified and Deleted loci in biliary tract cancer cell lines, Related to Figure 3. Significantly amplified and deleted loci across the 22 BTC cell lines determined using Illumina OmniExpress SNP arrays.

Amplified loci			
Cytoband	**q value**	**residual q value**	**wide peak boundaries**
12p12.1	2.74E-11	2.83E-10	chr12:24970589-25581258
12p12.2	0.00012196	0.0022211	chr12:20202918-21312923
12p11.1	0.0049466	0.034311	chr12:33940680-37927113
3q26.1	0.046253	0.046253	chr3:161570646-166861677
8q24.21	0.065588	0.065588	chr8:128129043-128408115
Deleted loci			
cytoband	**q value**	**residual q value**	**wide peak boundaries**
9p21.3	2.34E-21	2.34E-21	chr9:21865843-22451030
3p14.2	9.50E-11	9.50E-11	chr3:59029190-61549294
16q23.1	0.00018762	0.00018762	chr16:78129907-79628180
20p12.1	0.00039386	0.00039386	chr20:14295646-16034338
3q28	0.093074	0.093074	chr3:188605427-189356940

Table S4. Copy number variations in 22 BTC cell lines, Related to Figure 3. DNA copy-number was assessed using Illumina OmniExpress SNP arrays. Table is provided as a separate excel file.

Table S5. Mechanism of MAPK pathway deregulation in BTC cell lines, Related to Figures 5 and 6. MAPK pathway alterations were assessed using exome sequencing, copy number analysis or RNA-seq analysis.

Cell line	**MAPK pathway alteration**
OZ	*KRAS Q61L*
SNU869	*KRAS G12D*
TGBC14TKB	*KRAS G13C*
EGI1	*KRAS G12D*
G415	*KRAS G13D*
HUCCT1	*KRAS G12D*
KKUM213	*KRASG13C*
NOZ	*KRAS G12V, KRAS Amp*
SNU1196	*KRAS Amp*
SNU245	*KRAS Amp*
TGBC18TKB	*BRAF I581L, N582T*
Sk-Ch-A1	*BRAF D594T, RASA1 R726**
KKU-MO55	*MAP2K1 K57, FGFR1 overexpression*
TKKK	*WT*
SNU478	WT
TFK-1	WT
SNU1079	WT
TGBC2TKB	WT
SNU308	WT
HUH28	WT
MzChA2	WT
OCUG1	WT

Table S6. Short tandem repeat (STR) profiles of BTC cell lines, Related to Figure 1. STR profiling was performed on DNA isolated from each cell lines using the GenePrint 10 System.

	Cell Line	D5S818	D13S317	D7S820	D16S539	vWA	TH01	Amelogenin	TPOX	CSF1PO	D21S11	REFERENCE	STR match / result
1	**EGI-1**	13	11	9,13	13	17,19	6,9	X,Y	8,11	12,13	28, 33.2	Equivalent Ref #DSMZ ACC-385	EV=0.97
2	**G415**	12	8	11,12	12	16	7	X	11	12	32.2	Equivalent Ref RIKEN #RCB2640	EV=0.92
3	**HuCCT1**	12,13	11,13	10,11	11,12	18	7,10	X,Y	8	11,12	31	Equivalent Ref JCRB NIBIO #JCRB0425	EV=1.0
4	**HuH28**	9,12	9	10,11	9	17	9	X	8	9,12	30,33.2	Equivalent Ref JCRB NIBIO #JCRB0426	EV=0.96
5	**KKU-M055**	11	11	7,8	10,13	17,19	9	X	8	10,11	29,31	Equivilent Ref JCRB #JCRB1551	EV=1.0
6	**KKU-M213**	9	8,12	11	9,11	18	7	X	8	9,13	29	Equivilent Ref JCRB #JCRB1557	EV=1.0
7	**Sk-Ch-A1**	11,13	11,12	10	9,13	16,18	6	X	8	12,13	28	Not available	
8	**MzChA2**	10	12	11,12	11	15,17	8	X	11	12	28,30	Not available	
9	**NOZ**	13	8,12	10,11	9,11	19	7,9	X	8	11	30,31	Equivalent Ref JCRB NIBIO #JCRB1033	EV=0.91
10	**OCUG1**	10	8,11	10,11	9,13	16	7,*9.3	X	11	10,12	28,29	Equivalent Ref JCRB NIBIO #JCRB0191	EV=0.88
11	**OZ**	13,14	8,12	10	10	14,16	6,9	X,Y	9,11	11,12	29	Equivalent Ref JCRB NIBIO #JCRB1032	EV=1.0
12	**SNU245**	7	9,13	8,10	9,13	14,18	9	X	8	11	27,30	Equivalent Ref KCLB #00245	EV=0.96
13	**SNU308**	9	8	7,12	10,13	16	8	X	8	12	30,31	Equivalent Ref KCLB #00308	EV=1.0
14	**SNU478**	9,12	9,11	8,11	12	15,16	7	X	10,11	10,12	30	Equivalent Ref KCLB #00478	EV=1.0
15	**SNU869**	12	12	8,11	9	15	7,9	X	8,10	10	29,30	Equivalent Ref KCLB #00869	EV=1.0
16	**SNU1079**	10,13	8	8,12	10,11	16,18	8	X,Y	8	12	30	Equivalent Ref KCLB #01079	EV=1.0
17	**SNU1196**	11	9	8,11	11,12	14	7	X	10,11	10	30	Equivalent Ref KCLB #01196	EV=1.0
18	**TFK-1**	9,12	14	10	9	14,17	6	X,Y	8	10	30	Equivalent Ref DSMZ #ACC-344	EV=1.0
19	**TGBC2TKB**	11	8,11	9,13	9,11	14,17	9	X	8	14	-	Equivalent Ref RIKEN #RCB1130	EV=1.0
20	**TGBC14TKB**	12	12	10	9	14	6,7	X	8	12	28,30	Equivalent Ref RIKEN #RCB1186	EV=0.95
21	**TGBC18TKB**	14	8	11,12	9	18	9,9.3	X	8	14	31.2,32.2	Equivalent Ref RIKEN #RCB1169	EV=0.92
22	**TKKK**	13	8,12	10,11	11	16	6	X,Y	8	11	29	Equivalent Ref RIKEN #RCB1907	EV=0.96

Transparent Methods

Biliary tract cancer cell lines

The source and original publications describing the 22 BTC cell lines investigated are listed in **Supplemental Table 1**. All cell lines were maintained in Dulbecco's Modified Eagle Medium supplemented with 10% FBS, 1 mM HEPES buffer and penicillin/streptomycin (100 U/mL) at 37°C and 5% CO_2. Cell line authentication was performed using the GenePrint® 10 System (Promega, USA) (**Supplemental Table 6**). Cell lines were routinely tested for mycoplasma status by the MycoAlert Mycoplasma Detection Kit (Lonza) and confirmed to be negative.

Exome-capture sequencing: Exome-capture was performed using the Agilent SureSelect XT Human All Exon v5 and 100 bp paired-end read sequencing performed on an Illumina HiSeq 2000 System. Raw FASTQ paired-end reads were aligned against the human hg19 reference sequence using the Burrows-Wheeler Alignment (BWA) tool (Li and Durbin, 2009). Variants were annotated against databases of known human germline variations (dbSNP, build 135, SAO = 1), 1000 Genomes Project database (build 20110521), Mills *et al* dataset of small insertions and deletions (Mills et al., 2011) and germline variants detected in 114 normal colorectal tissues analyzed in our laboratories. Somatic mutation signatures were generated using the "SomaticSignatures" package. Significantly mutated genes determined in MutSig.

RNA-seq analysis: Total RNA was extracted from cell pellets using the High Pure RNA Isolation Kit (Roche, Basel, Switzerland) as per manufacturer's protocol, which included a DNase I step. cDNA synthesis, library preparation of six indexed samples and RNA-Seq analysis was performed on an Illumina HiSeq2000 to a minimum depth of >20 million 100bp single end reads. Raw reads were assessed for good quality using the FASTQC software. Alignment of transcript sequences to the human reference genome (build hg19) was performed using the TopHat (2.1.0) software with default parameters (Trapnell et al., 2012). Gene regions were identified based on alignments of the RefSeq human database by the UCSC genome browser (hg19). Normalized gene expression values were calculated by counting aligning reads per kilobase per million reads mapped (RPKM) and counts per million (CPM). Absence of gene expression was defined as a RPKM value of <1. *FGFR2* fusion transcripts were investigated by visualisation of aligned transcripts using the Integrative Genomics Viewer v2.4 (Broad Institute, Cambridge MA, USA) (Robinson et al., 2011).

DNA copy number analysis: DNA copy number was assessed using Illumina HumanOmniExpress-24 BeadChip and analysed using GenomeStudio (Illumina). SNPs showing germline alterations, based on 637 normal samples, were excluded. DNA copy-number segmentation and absolute copy number estimates was performed using OncoSNPv2.18 (Yau et al., 2010), and significantly altered regions identified using GISTIC2.0 (van Dyk et al., 2013).

Cell block generation and Immunohistochemistry (IHC): Cultured cell lines (minimum $1x10^7$) were pelleted and coagulated in human plasma (150 µL) and bovine thrombin (1units/µL) for 5 mins (Pfizer, New York, NY, USA), fixed in 10% formalin, and paraffin embedded. p53 was detected using an anti-p53 antibody (DO-7 clone, Novocastra, 1:100), followed by signal detection using an enzyme-conjugated multimer secondary antibody, UltraView Universal DAB detection kit (Ventana), using standard protocols.

Luciferase reporter assays: Cell lines seeded in 96 well plates were transfected with 0.1 µg/well of the β-catenin-TCF reporter plasmid (TOPFLASH,) or control plasmid (FOPFLASH) (van de Wetering et al., 1997) using Lipofectamine 2000 (0.2µL/well, Thermo Fisher Scientific). *Renilla*-TK (0.04 µg/well) was used to control for transfection efficiency. After 48h, cells were harvested in passive lysis buffer (Promega), and luciferase activity measured using the Dual Luciferase Reporter Assay System (Promega) on a Spectromax L Microplate reader (Molecular Devices).

MTS assays

Cell proliferation was determined by MTS (3-(4,5-dimethyl-2-yl)-5-(3-carboxymethoxyphenyl)-2-(4-sulfophenyl)-2H-tetrazolium, inner salt) assay using the CellTiter 96® AQ_{ueous} One Solution Assay kit (Promega) as per manufacturer's instructions.

Organoid proliferation
Cells from cholangiocarcinoma organoids 1T, 9T and 24T were plated (1.2 x 10^3 / well) were cultured for 4 days as described previously (Saito et al., 2019). Organoids were treated with AG-120 (Cayman chemical) for 6 days and cell viability determined by WST assay using the Cell Counting Kit-8 (Dojindo).

Western blotting
20-40 μg of protein was resolved under denaturing conditions (SDS-PAGE) and transferred to PVDF membrane. Membranes were blocked in Odyssey blocking buffer (Li-Cor Bioscience) and probed with anti-pERK1/2 (Thr202/Tyr 204, cat no 4370, Cell Signaling Technology, Danvers MA), anti-ERK1/2 (Cat no: 9107, Cell Signaling), anti-pCRAF (Ser338, Cat no: 9427, Cell Signaling), anti-FGFR1 (Cat no. 9740 Cell Signaling), anti-β-actin (Cat no. A5316, Sigma-Aldrich, MO, USA) or anti-β-tubulin (ab6046, Abcam, Cambridge UK) at room temperature for 1h. Anti-rabbit or mouse secondary antibodies were incubated at room temperature 1h. The infrared fluorescence image was obtained using Odyssey infrared imaging system (Li-Cor Bioscience).

Xenograft studies
Animal experiments were approved by the Austin Health Animal Ethics Committee. 1-2 x 10^6 cells comprising 100 µL of cells (in PBS) and 100 µl Matrigel (Corning, NY, USA) were subcutaneously injected into the right and left flanks of male Balb/*c* nu/nu mice. Tumours were grown for a maximum of 4 weeks, or until the combined tumour size reached 1 cm^3. Resected tumours were fixed in 10% formalin, and stained with haematoxylin and eosin. For erdafitinib experiments, mice were treated daily for 18 days with 20 mg/kg erdafitinib (MedChem Express, NJ, USA) or vehicle (20% hydroxypropyl b cyclodextrin, Sigma Aldrich) by oral gavage. Tumour growth was measured every second day by caliper.

Data and software availablity
RNA-seq data is accessible via the Gene Expression Omnibus, with accession number GSE138772 (https://www.ncbi.nlm.nih.gov/geo/query/acc.cgi?acc=GSE138772).

Supplemental References

Li, H., and Durbin, R. (2009). Fast and accurate short read alignment with Burrows-Wheeler transform. Bioinformatics *25*, 1754-1760.

Mills, R.E., Pittard, W.S., Mullaney, J.M., Farooq, U., Creasy, T.H., Mahurkar, A.A., Kemeza, D.M., Strassler, D.S., Ponting, C.P., Webber, C., et al. (2011). Natural genetic variation caused by small insertions and deletions in the human genome. Genome Res *21*, 830-839.

Robinson, J.T., Thorvaldsdottir, H., Winckler, W., Guttman, M., Lander, E.S., Getz, G., and Mesirov, J.P. (2011). Integrative genomics viewer. Nat Biotechnol *29*, 24-26.

Saito, Y., Muramatsu, T., Kanai, Y., Ojima, H., Sukeda, A., Hiraoka, N., Arai, E., Sugiyama, Y., Matsuzaki, J., Uchida, R., et al. (2019). Establishment of Patient-Derived Organoids and Drug Screening for Biliary Tract Carcinoma. Cell reports *27*, 1265-1276 e1264.

Trapnell, C., Roberts, A., Goff, L., Pertea, G., Kim, D., Kelley, D.R., Pimentel, H., Salzberg, S.L., Rinn, J.L., and Pachter, L. (2012). Differential gene and transcript expression analysis of RNA-seq experiments with TopHat and Cufflinks. Nature protocols *7*, 562-578.

van de Wetering, M., Cavallo, R., Dooijes, D., van Beest, M., van Es, J., Loureiro, J., Ypma, A., Hursh, D., Jones, T., Bejsovec, A., et al. (1997). Armadillo coactivates transcription driven by the product of the Drosophila segment polarity gene dTCF. Cell *88*, 789-799.

van Dyk, E., Reinders, M.J., and Wessels, L.F. (2013). A scale-space method for detecting recurrent DNA copy number changes with analytical false discovery rate control. Nucleic Acids Res *41*, e100.

Yau, C., Mouradov, D., Jorissen, R.N., Colella, S., Mirza, G., Steers, G., Harris, A., Ragoussis, J., Sieber, O., and Holmes, C.C. (2010). A statistical approach for detecting genomic aberrations in heterogeneous tumor samples from single nucleotide polymorphism genotyping data. Genome Biol *11*, R92.